4. Katsuno M, Adachi H, Tanaka F, Sobue G. Spinal and bulbar muscular atrophy: ligand-dependent pathogenesis and therapeutic perspectives. J Mol Med 2004;82:298–307.
5. Fischbeck KH. Kennedy disease. J Inherit Metab Dis 1997;20: 152–158.
6. Katsuno M, Adachi H, Waza M, et al. Pathogenesis, animal models and therapeutics in spinal and bulbar muscular atrophy (SBMA). Exp Neurol 2006;200:8–18.
7. Atsuta N, Watanabe H, Ito M, et al. Natural history of spinal and bulbar muscular atrophy (SBMA): a study of 223 Japanese patients. Brain 2006;129:1446–1455.
8. La Spada AR, Wilson EM, Lubahn DB, et al. Androgen receptor gene mutations in X-linked spinal and bulbar muscular atrophy. Nature 1991;352:77–79.
9. Tanaka F, Doyu M, Ito Y, et al. Founder effect in spinal and bulbar muscular atrophy (SBMA). Hum Mol Genet 1996;5: 1253–1257.
10. Andrew SE, Goldberg YP, Hayden MR. Rethinking genotype and phenotype correlations in polyglutamine expansion disorders. Hum Mol Genet 1997;6:2005–2010.
11. Doyu M, Sobue G, Mukai E, et al. Severity of X-linked recessive bulbospinal neuronopathy correlates with size of the tandem CAG repeat in androgen receptor gene. Ann Neurol 1992; 32:707–710.
12. Shimada N, Sobue G, Doyu M, et al. X-linked recessive bulbospinal neuronopathy: clinical phenotypes and CAG repeat size in androgen receptor gene. Muscle Nerve 1995;18: 1378–1384.
13. Zoghbi HY, Orr HT. Glutamine repeats and neurodegeneration. Annu Rev Neurosci 2000;23:217–247.
14. Ross CA. Polyglutamine pathogenesis: emergence of unifying mechanisms for Huntington's disease and related disorders. Neuron 2002;35:819–822.
15. Gatchel JR, Zoghbi HY. Diseases of unstable repeat expansion: mechanisms and common principles. Nat Rev Genet 2005;6: 743–755.
16. Adachi H, Katsuno M, Minamiyama M, et al. Widespread nuclear and cytoplasmic accumulation of mutant androgen receptor in SBMA patients. Brain 2005;128:659–670.
17. Banno H, Adachi H, Katsuno M, et al. Mutant androgen receptor accumulation in spinal and bulbar muscular atrophy scrotal skin: a pathogenic marker. Ann Neurol 2006;59: 520–526.
18. Sobue G, Doyu M, Kachi T, et al. Subclinical phenotypic expressions in heterozygous females of X-linked recessive bulbospinal neuronopathy. J Neurol Sci 1993;117:74–78.
19. Schmidt BJ, Greenberg CR, Allingham-Hawkins DJ, Spriggs EL. Expression of X-linked bulbospinal muscular atrophy (Kennedy disease) in two homozygous women. Neurology 2002;59:770–772.
20. Katsuno M, Adachi H, Kume A, et al. Testosterone reduction prevents phenotypic expression in a transgenic mouse model of spinal and bulbar muscular atrophy. Neuron 2002;35: 843–854.
21. Katsuno M, Adachi H, Doyu M, et al. Leuprorelin rescues polyglutamine-dependent phenotypes in a transgenic mouse model of spinal and bulbar muscular atrophy. Nat Med 2003; 9:768–773.
22. Takeyama K, Ito S, Yamamoto A, et al. Androgen-dependent neurodegeneration by polyglutamine-expanded human androgen receptor in Drosophila. Neuron 2002;35:855–864.
23. Chevalier-Larsen ES, O'Brien CJ, Wang H, et al. Castration restores function and neurofilament alterations of aged symptomatic males in a transgenic mouse model of spinal and bulbar muscular atrophy. J Neurosci 2004;24:4778–4786.
24. Shimohata T, Kimura T, Nishizawa M, et al. Five year follow up of a patient with spinal and bulbar muscular atrophy treated with leuprorelin. J Neurol Neurosurg Psychiatry 2004;75: 1206–1207.
25. Wilson AC, Meethal SV, Bowen RL, Atwood CS. Leuprolide acetate: a drug of diverse clinical applications. Expert Opin Investig Drugs 2007;16:1851–1863.
26. Pocock SJ, Simon R. Sequential treatment assignment with balancing for prognostic factors in the controlled clinical trial. Biometrics 1975;31:103–115.
27. Niijima T, Aso Y, Akaza H, et al. [Clinical phase I and phase II study on a sustained release formulation of leuprorelin acetate (TAP-144-SR), an LH-RH agonist, in patients with prostatic carcinoma. Collaborative++ Studies on Prostatic Carcinoma by the Study Group for TAP-144-SR.]. Hinyokika Kiyo 1990; 36:1343–1360.
28. Plosker GL, Brogden RN. Leuprorelin. A review of its pharmacology and therapeutic use in prostatic cancer, endometriosis and other sex hormone-related disorders. Drugs 1994;48: 930–967.
29. Ohashi Y, Tashiro K, Itoyama Y, et al. [Study of functional rating scale for amyotrophic lateral sclerosis: revised ALSFRS(ALSFRS-R) Japanese version]. No To Shinkei 2001; 53:346–355.
30. Chahin N, Klein C, Mandrekar J, Sorenson E. Natural history of spinal-bulbar muscular atrophy. Neurology 2008;70: 1967–1971.
31. Morin LG. Creatine kinase: re-examination of optimum reaction conditions. Clin Chem 1977;23:1569–1575.
32. Logemann JA, Pauloski BR, Rademaker AW, et al. Temporal and biomechanical characteristics of oropharyngeal swallow in younger and older men. J Speech Lang Hear Res 2000;43: 1264–1274.
33. Logemann JA. Evaluation and treatment of swallowing disorders. 2nd ed. Austin, TX: Pro-Ed, 1998.
34. Trottier Y, Lutz Y, Stevanin G, et al. Polyglutamine expansion as a pathological epitope in Huntington's disease and four dominant cerebellar ataxias. Nature 1995;378:403–406.
35. Terao S, Sobue G, Hashizume Y, et al. Age-related changes in human spinal ventral horn cells with special reference to the loss of small neurons in the intermediate zone: a quantitative analysis. Acta Neuropathol 1996;92:109–114.
36. Suzuki K, Katsuno M, Banno H, et al. CAG repeat size correlates to electrophysiological motor and sensory phenotypes in SBMA. Brain 2008;131:229–239.
37. Nishie M, Mori F, Yoshimoto M, et al. A quantitative investigation of neuronal cytoplasmic and intranuclear inclusions in the pontine and inferior olivary nuclei in multiple system atrophy. Neuropathol Appl Neurobiol 2004;30:546–554.
38. Tanaka F, Reeves MF, Ito Y, et al. Tissue-specific somatic mosaicism in spinal and bulbar muscular atrophy is dependent on CAG-repeat length and androgen receptor–gene expression level. Am J Hum Genet 1999;65:966–973.
39. Takeuchi Y, Katsuno M, Banno H, et al. Walking capacity evaluated by the 6-minute walk test in spinal and bulbar muscular atrophy. Muscle Nerve 2008;38:964–971.
40. Fowler JE Jr, Gottesman JE, Reid CF, et al. Safety and efficacy of an implantable leuprolide delivery system in patients with advanced prostate cancer. J Urol 2000;164:730–734.
41. Taylor JP, Hardy J, Fischbeck KH. Toxic proteins in neurodegenerative disease. Science 2002;296:1991–1995.
42. Orr HT, Zoghbi HY. Trinucleotide repeat disorders. Annu Rev Neurosci 2007;30:575–621.
43. Zhou ZX, Lane MV, Kemppainen JA, et al. Specificity of ligand-dependent androgen receptor stabilization: receptor domain interactions influence ligand dissociation and receptor stability. Mol Endocrinol 1995;9:208–218.

44. Jacob P, Kahrilas PJ, Logemann JA, et al. Upper esophageal sphincter opening and modulation during swallowing. Gastroenterology 1989;97:1469–1478.
45. Lazarus CL, Logemann JA, Rademaker AW, et al. Effects of bolus volume, viscosity, and repeated swallows in nonstroke subjects and stroke patients. Arch Phys Med Rehabil 1993;74: 1066–1070.
46. Williams RB, Grehan MJ, Hersch M, et al. Biomechanics, diagnosis, and treatment outcome in inflammatory myopathy presenting as oropharyngeal dysphagia. Gut 2003;52: 471–478.
47. Ertekin C, Aydogdu I, Yuceyar N, et al. Pathophysiological mechanisms of oropharyngeal dysphagia in amyotrophic lateral sclerosis. Brain 2000;123(pt 1):125–140.
48. A double-blind placebo-controlled clinical trial of subcutaneous recombinant human ciliary neurotrophic factor (rHCNTF) in amyotrophic lateral sclerosis. ALS CNTF Treatment Study Group. Neurology 1996;46:1244–1249.
49. Leuprolide versus diethylstilbestrol for metastatic prostate cancer. The Leuprolide Study Group. N Engl J Med 1984;311: 1281–1286.
50. Higano CS. Side effects of androgen deprivation therapy: monitoring and minimizing toxicity. Urology 2003;61:32–38.
51. Dejager S, Bry-Gauillard H, Bruckert E, et al. A comprehensive endocrine description of Kennedy's disease revealing androgen insensitivity linked to CAG repeat length. J Clin Endocrinol Metab 2002;87:3893–3901.

Human Molecular Genetics, 2009, Vol. 18, No. 5 **898–910**
doi:10.1093/hmg/ddn419
Advance Access published on December 9, 2008

17-DMAG ameliorates polyglutamine-mediated motor neuron degeneration through well-preserved proteasome function in an SBMA model mouse

Keisuke Tokui[1,†], Hiroaki Adachi[1,*,†], Masahiro Waza[1], Masahisa Katsuno[1,2], Makoto Minamiyama[1], Hideki Doi[1], Keiji Tanaka[3], Jun Hamazaki[4], Shigeo Murata[4], Fumiaki Tanaka[1] and Gen Sobue[1,*]

[1]Department of Neurology, Nagoya University Graduate School of Medicine, 65 Tsurumai-cho, Showa-ku, Nagoya 466-8550, Japan, [2]Institute for Advanced Research, Nagoya University, 65 Tsurumai-cho, Showa-ku, Nagoya 466-8550, Japan, [3]Laboratory of Frontier Science, Core Technology and Research Center, Tokyo Metropolitan Institute of Medical Science, Bunkyo-ku, Tokyo 113-8613, Japan and [4]Laboratory of Protein Metabolism, Graduate School of Pharmaceutical Sciences, University of Tokyo, 7-3-1 Hongo, Bunkyo-ku, Tokyo 113-0033, Japan

Received October 1, 2008; Revised November 13, 2008; Accepted December 5, 2008

The ubiquitin–proteasome system (UPS) is the principal protein degradation system that tags and targets short-lived proteins, as well as damaged or misfolded proteins, for destruction. In spinal and bulbar muscular atrophy (SBMA), the androgen receptor (AR), an Hsp90 client protein, is such a misfolded protein that tends to aggregate in neurons. Hsp90 inhibitors promote the degradation of Hsp90 client proteins via the UPS. In a transgenic mouse model of SBMA, we examined whether a functioning UPS is preserved, if it was capable of degrading polyglutamine-expanded mutant AR, and what might be the therapeutic effects of 17-(dimethylaminoethylamino)-17-demethoxygeldanamycin (17-DMAG), an oral Hsp90 inhibitor. Ubiquitin-proteasomal function was well preserved in SBMA mice and was even increased during advanced stages when the mice developed severe phenotypes. Administration of 17-DMAG markedly ameliorated motor impairments in SBMA mice without detectable toxicity and reduced amounts of monomeric and nuclear-accumulated mutant AR. Mutant AR was preferentially degraded in the presence of 17-DMAG in both SBMA cell and mouse models when compared with wild-type AR. 17-DMAG also significantly induced Hsp70 and Hsp40. Thus, 17-DMAG would exert a therapeutic effect on SBMA via preserved proteasome function.

INTRODUCTION

Polyglutamine (polyQ) diseases are inherited neurodegenerative disorders caused by the expansion of trinucleotide repeats in the causative genes (1). One of these is spinal and bulbar muscular atrophy (SBMA), characterized by premature muscular exhaustion, progressive muscular weakness, atrophy and fasciculation in bulbar and limb muscles (2). In SBMA, a CAG repeat with 14–32 CAGs expands to 40–62 CAGs in the first exon of the androgen receptor (AR) gene (3). Pathological findings of SBMA are lower motor neuronal loss (4) and diffuse nuclear accumulations and nuclear inclusions (NIs) of polyQ-expanded mutant AR in the residual motor neurons in the brainstem and spinal cord as well as in some other visceral organs (5).

Heat shock protein 90 (Hsp90), a cytosolic molecular chaperone, is involved in the maturation and activation of a number of proteins, known as client proteins. Hsp90 client proteins comprise numerous oncoproteins (6) and steroid receptors, including AR (7). Hsp90 inhibitors enhance the proteasomal degradation of

*To whom correspondence should be addressed. Tel: +81 52-744-2385; Fax: +81 52-744-2384; Email: hadachi@med.nagoya-u.ac.jp; sobueg@med.nagoya-u.ac.jp
†The authors wish it to be known that, in their opinion, the first two authors should be regarded as joint First Authors.

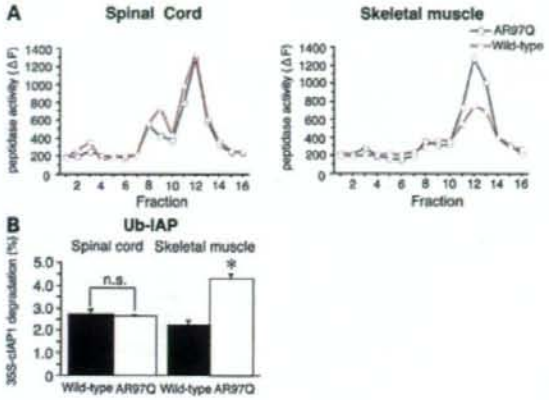

Figure 1. Protein-degrading activity of proteasomes. (**A**) Chymotryptic activity of 26S proteasomes in AR-97Q (SBMA) and AR-24Q (wild-type) mice. (**B**) Ubiquitin-dependent degradation of 35S-labeled cIAP1 in AR-24Q (wild-type) and AR-97Q mice. Data are mean ± SE from triplicate experiments. $^*P < 0.005$.

the Hsp90 client proteins, particularly of their mutant versions (8). Additionally, Hsp90 inhibitors also function as Hsp inducers (9). Therefore, numerous oncoproteins belonging to the Hsp90 client protein family are selectively degraded in the ubiquitin–proteasome system (UPS) by Hsp90 inhibitors. 17-(dimethylaminoethylamino)-17-demethoxy-geldanamycin (17-DMAG; NSC707545), a potent Hsp90 inhibitor, is now under clinical trials as a novel molecular-targeted agent for a wide range of malignancies (10). Recently, we explored the possibility of using 17-allylamino-17-demethoxygeldanamycin (17-AAG; NSC-330507), another Hsp90 inhibitor, as a therapeutic agent for SBMA and found that 17-AAG inhibits nuclear accumulation of the mutant AR protein, leading to marked amelioration of the motor phenotype of the transgenic mouse model of SBMA (AR-97Q mice) without detectable toxicity (11). 17-DMAG is a more potent derivative of 17-AAG (12,13), is more water soluble than 17-AAG and can be administered orally (14), thus possibly making it a more feasible long-term therapeutic agent for treating SBMA.

Hsp90 inhibitor-induced client protein degradation requires a well-preserved proteasome function; however, the question of whether the UPS is impaired in patients with polyQ diseases has been raised with respect to this UPS-dependent therapy (15). It is generally considered that the UPS is involved in polyQ diseases, as many components of the UPS and molecular chaperones are known to co-localize with polyQ-containing NIs (16,17). Nevertheless, previous studies using proteasome assays performed in cultured cell and mouse models of polyQ diseases have not shown consistent results; the UPS was impaired in some (18–24) and preserved in others (25–29). If the UPS is irreversibly damaged in patients and animal models of polyQ diseases, Hsp90 inhibitors cannot exert their pharmacological effects. Thus, it is important to assess whether the UPS is impaired, particularly in *in vivo* models of polyQ diseases with advanced phenotypic expressions. In this study, we employed multiple assessments to investigate whether the UPS function is preserved in transgenic AR-97Q SBMA mice and examined the effects of 17-DMAG on the phenotypic expression of SBMA in these mice.

RESULTS

Proteasomal proteolytic activity is preserved in AR-97Q mice with advanced phenotypes

To investigate proteasome functions, the chymotryptic activity of the proteasome was examined in AR-24Q (wild-type AR) and AR-97Q (mutant AR) mice at an advanced stage (16 weeks) (30). Most 16-week-old AR-97Q mice developed the severe phenotype. Chymotryptic activities of the 26S proteasomes in the AR-97Q mice were similar to wild-type in the spinal cord (Fig. 1A, left) and increased with respect to wild-type in skeletal muscle (Fig. 1A, right). We also examined ubiquitin-dependent proteolytic activity using 35S-labeled ubiquitinated cIAP1, a ubiquitin ligase that catalyzes its own ubiquitination for degradation. The levels of ubiquitin-dependent degradation in spinal cord of AR-97Q mice were not significantly different from wild-type (Fig. 1B, left); in skeletal muscle, however, degradation was higher in the AR-97Q mice than in the wild-type mice (Fig. 1B, right). These assays indicate that proteasomal function in AR-97Q mice with severe phenotypes was preserved in the spinal cord and was enhanced in skeletal muscle.

Proteasomal function in Ub^{G76V}-GFP/AR-97Q reporter mice is preserved

The Ub^{G76V}-GFP mouse was developed as an *in vivo* reporter of UPS function (31). They express an N-terminal ubiquitin mutant (Ub^{G76V}) in frame with enhanced green fluorescent protein (32). As the reporter is rapidly processed and degraded by the UPS, steady-state levels of Ub^{G76V}-GFP are very low under wild-type conditions, but accumulate when the UPS is impaired. We evaluated levels of Ub^{G76V}-GFP in spinal cord and skeletal muscle lysates of double transgenic, Ub^{G76V}-GFP/AR-97Q and Ub^{G76V}-GFP/AR-24Q mice (see Supplementary Material). Immunoblot analyses showed that Ub^{G76V}-GFP in the AR-97Q mice was increased in the spinal cord (30%) and skeletal muscle (85%) compared with AR-24Q mice (Fig. 2A). These results were well correlated

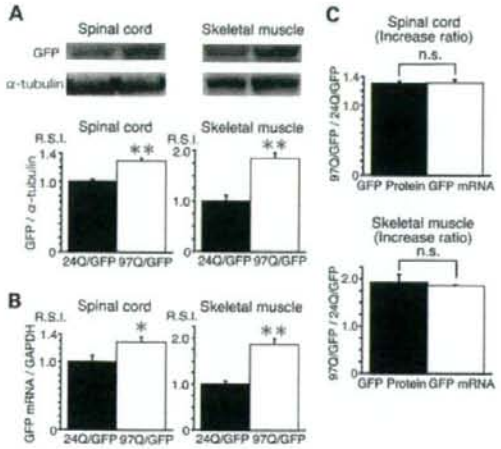

Figure 2. Ub^{G76V}-GFP reporter expression levels in the spinal cord and skeletal muscle of 16-week-old AR-24Q and AR-97Q mice. (**A**) Quantification of Ub^{G76V}-GFP protein levels by western blot relative to α-tubulin in the spinal cord and skeletal muscle of Ub^{G76V}-GFP/AR-24Q and Ub^{G76V}-GFP/AR-97Q mice. (**B**) Quantification of Ub^{G76V}-GFP mRNA levels relative to GAPDH by real-time RT–PCR analysis in the spinal cord and skeletal muscle of Ub^{G76V}-GFP/AR-24Q and Ub^{G76V}-GFP/AR-97Q mice. Values in (A) and (B) are expressed as mean ± SE, $n = 6$; $^{*}P < 0.05$; $^{**}P < 0.0005$. (**C**) The relative increases in Ub^{G76V}-GFP protein and mRNA levels in Ub^{G76V}-GFP/AR-24Q and Ub^{G76V}-GFP/AR-97Q mice. $n = 6$.

with those of anti-GFP immunohistochemical-stained tissue sections (compare with Supplementary Material, Fig. S1A and C).

To assess whether the increases in reporter levels reflect UPS function or reporter mRNA expression levels, we quantified mRNA levels of Ub^{G76V}-GFP by real-time RT–PCR and noted increases in Ub^{G76V}-GFP mRNA levels in Ub^{G76V}-GFP/AR-97Q mice compared with those in Ub^{G76V}-GFP/AR-24Q mice (Fig. 2B). The increases in protein levels were very similar to those in mRNA levels (Fig. 2C), strongly indicating that the increases in reporter proteins in the spinal cord and muscle were due to increased expressions of reporter protein mRNAs and that UPS function is well preserved in AR-97Q mice even in their advanced stage. Furthermore, *in situ* hybridization (Supplementary Material) also demonstrated an increase in Ub^{G76V}-GFP reporter mRNA levels in the spinal motor neurons and skeletal muscle of AR-97Q mice compared with those of AR-24Q mice (Supplementary Material, Fig. S1B and D). This increase was comparable to that seen in anti-GFP immunohistochemical staining (Supplementary Material, Fig. S1A and E), indicating again that the increased protein is due to increased reporter mRNA and that UPS function in the motor neurons of AR-97Q mice is well preserved.

Expression of proteasomal mRNAs and proteins are preserved in AR-97Q mice

To verify the protein expression levels of proteasomal subunits in advanced stage AR-24Q and AR-97Q mice, immunoblot analyses with various anti-proteasomal subunit antibodies

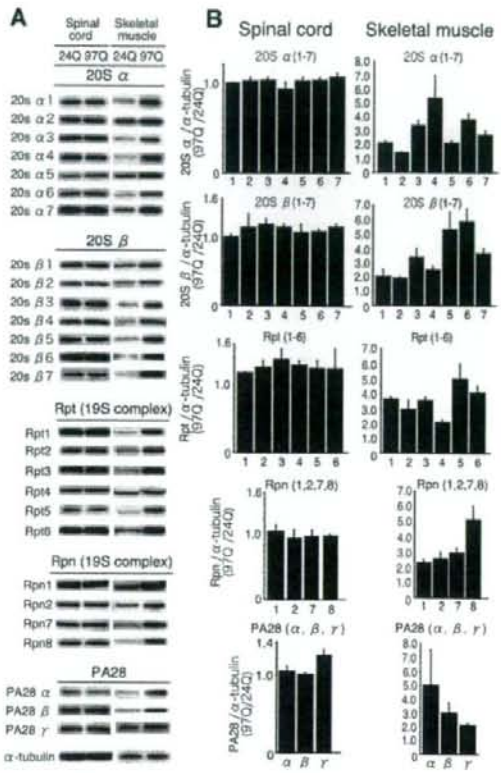

Figure 3. The protein expression levels of proteasome subunits in 16-week-old AR-97Q and AR-24Q mice. (**A**) Immunoblot analyses of various proteasome subunits in spinal cord and skeletal muscle. (**B**) Quantification of the ratios of subunit levels in AR-97Q versus AR-24Q mice.

were conducted in spinal cord and muscle lysates (Supplementary Material). The levels of all proteasome subunits, including those in the 20S proteasome (α1-7, β1-7), the 19S regulatory particles (Rpt1-6, Rpn1,2,7,8) and the proteasome activators (PA28α,β,γ) in the spinal cord of AR-97Q mice, were similar to those in the AR-24Q mice (Fig. 3A and B). On the other hand, protein levels of all proteasomal subunits in the skeletal muscle of the AR-97Q mice were higher than those in the AR-24Q mice (Fig. 3A and B). Representative immunohistochemical analyses also revealed the elevated expression levels of proteasomal subunits 20S α1, α4, α5, α7, β2 and 19S Rpt3 in the skeletal muscle of AR-97Q versus AR-24Q mice (Supplementary Material, Fig. S2) and no differences in the patterns of proteasomal subunit stainings in the spinal anterior horn cells of the AR-24Q and AR-97Q mice (Supplementary Material, Fig. S2). Likewise, quantitative real-time RT–PCR analysis showed that levels of mRNA encoding representative proteasomal subunits in the spinal cords of AR-97Q mice were similar to those in AR-24Q mice (Supplementary Material, Fig. S3A), whereas mRNA levels of the same proteasomal subunits were

increased in AR-97Q skeletal muscle compared with AR-24Q (Supplementary Material, Fig. S3B). Thus, the increases in proteasomal subunit mRNAs were well correlated to those in proteasomal subunit proteins, to increased chymotryptic activity and to ubiquitin-dependent degradation of ^{35}S-labeled cIAP1 in AR-97Q skeletal muscle. Furthermore, there was no difference in the proteasomal subunit expression levels in the spinal anterior horn cells of the AR-24Q and AR-97Q mice. Next we evaluated the co-localization of proteasomal subunits and mutant AR in AR-97Q mice. Double-immunofluorescence staining with anti-20S proteasome α1 or α7 subunit and mouse anti-expanded polyQ (1C2) antibodies revealed that the 20S proteasome α1 or α7 subunits (Supplementary Material, Fig. S4A, D, G and J) and mutant AR (Supplementary Material, Fig. S4B, E, H and K) were partially co-localized in the nuclei (Supplementary Material, Fig. S4C, F, I and L) of the spinal anterior horn neurons and skeletal muscle cells of the AR-97Q mice, suggesting that the proteasomal subunits co-exist with mutant AR and exert their function in the AR-97Q mice. Moreover, the expression levels of 20S proteasome α1 and α7 subunits appeared to be elevated in the 1C2-positive muscle fibers (Supplementary Material, Fig. S4I and L), and those signals were unchanged in spinal motor neurons (Supplementary Material, Fig. S4A–F), indicating that the increase observed in the skeletal muscle is due to direct effects of the mutant AR on the skeletal muscle. Taken together, the results demonstrate there was no significant impairment of UPS activity in the AR-97Q mice with severe phenotypes.

17-DMAG preferentially reduces the amount of the polyQ-expanded mutant AR by integrating into the Hsp90 chaperone complex

To examine the efficacy of 17-DMAG to degrade mutant polyQ-expanded AR, we treated SH-SY5Y cells highly expressing either AR-24Q or AR-97Q with 17-DMAG or vehicle (DMSO). Although the anti-AR immunoblot showed a dose-dependent decline in both wild-type and mutant AR expression in response to 17-DMAG (Fig. 4A), the decrease in monomeric mutant AR (70% at 100 nM 17-DMAG) was significantly more than in wild-type (29%; Fig. 4B), suggesting that mutant AR is more selectively degraded by 17-DMAG than is wild-type. In addition, the pharmacological effect of 17-DMAG was three times as strong as that of 17-AAG (Fig. 4C and D). 17-DMAG also significantly increased the expression of both Hsp70 and Hsp40, but only slightly increased Hsp90 expression (Fig. 4A and B). There were no significant differences, however, in the levels of Hsp70 and Hsp40 induction in cells transfected with the wild-type or mutant AR (Fig. 4B). There was also no difference in cell viability between wild-type- and mutant AR-transfected cells (data not shown). These data indicate that 17-DMAG preferentially degrades the mutant AR protein without cellular toxicity.

We next examined the status of the Hsp90 chaperone complex in mutant AR-expressing cultured cells treated with 17-DMAG. After 30 min of 17-DMAG treatment, immunoprecipitation with an AR-specific antibody showed that Hsp90 chaperone complex-associated Hop was markedly increased and p23 decreased in a dose-dependent manner (Fig. 4E), suggesting that treatment with 17-DMAG shifted the AR-Hsp90 chaperone complex from a mature stabilizing form with p23 to a proteasome-targeting form with Hop (33). This finding is consistent with our previous report using 17-AAG (11). Immunoprecipitation with the AR-specific antibody showed that the mutant AR was more strongly ubiquitinated in cells treated with 17-DMAG in the presence of the proteasome inhibitor MG132 than those treated with DMSO alone (Fig. 4F). In addition, the degradation of mutant AR-97Q by 17-DMAG was completely suppressed by MG132 (Fig. 4F, bottom row). These results suggest that following treatment with 17-DMAG, the Hsp90 chaperone complex and client proteins are targeted for degradation via the UPS as previously reported (34,35).

The mutant AR was shown to be degraded only when Hsp70 was induced (36). However, mutant AR was markedly decreased following treatment with 17-DMAG, even when the induction of Hsp70 was blocked by a small interfering RNA (Fig. 4G and H). This suggests that 17-DMAG contributes to the preferential degradation of mutant AR through Hsp90 chaperone complex formation and subsequent proteasome-dependent degradation, even without induction of Hsp70.

17-DMAG ameliorates phenotypic expression of the SBMA transgenic mouse

We administrated 17-DMAG from age 5 to 25 weeks at doses of 1.0 or 10 mg/kg to male AR-97Q or AR-24Q mice and examined various neurological and behavioral parameters. The disease progression of AR-97Q mice treated with 10 mg/kg 17-DMAG (Tg-10) was significantly ameliorated and that of mice treated with 1.0 mg/kg 17-DMAG (Tg-1) mildly ameliorated (Fig. 5A–D). The untreated male mice (Tg-0) showed motor impairment assessed by the Rotarod task as early as 9 weeks after birth, whereas the Tg-10 mice showed initial impairment only 16 weeks after birth and with less deterioration than the Tg-0 mice ($P<0.005$, Fig. 5A). The locomotor cage activity of the Tg-0 mice was also significantly decreased at 10 weeks compared with the Tg-10 mice ($P < 0.005$, Fig. 5B). The Tg-0 mice lost weight significantly earlier and more profoundly than the Tg-10 mice ($P < 0.005$, Fig. 5C). 17-DMAG also significantly prolonged the survival rate of both the Tg-1 ($P < 0.05$) and Tg-10 ($P < 0.0001$) mice compared with the Tg-0 mice (Fig. 5D). Although both the Tg-10 and Tg-1 mice showed ameliorated phenotypic expressions, the Tg-10 mice were better than the Tg-1 mice in all parameters, suggesting that the improved motor phenotype depended on drug efficacy. In addition, the Tg-0 mice showed motor weakness, taking shorter steps and dragging their legs, whereas the Tg-10 mice showed almost normal ambulation (Fig. 5E and F).

To evaluate the toxicity of 17-DMAG, we examined blood samples from 25-week-old mice treated with 10 mg/kg 17-DMAG for 20 weeks (Supplementary Material). Measurements of aspartate aminotransferase, alanine aminotransferase, blood urea nitrogen and serum creatinine demonstrated that 17-DMAG resulted in neither liver nor renal dysfunction in the AR-97Q mice at the dose of 10 mg/kg (Supplementary Material, Fig. S5). Additionally, no treated mice were infertile (data not shown).

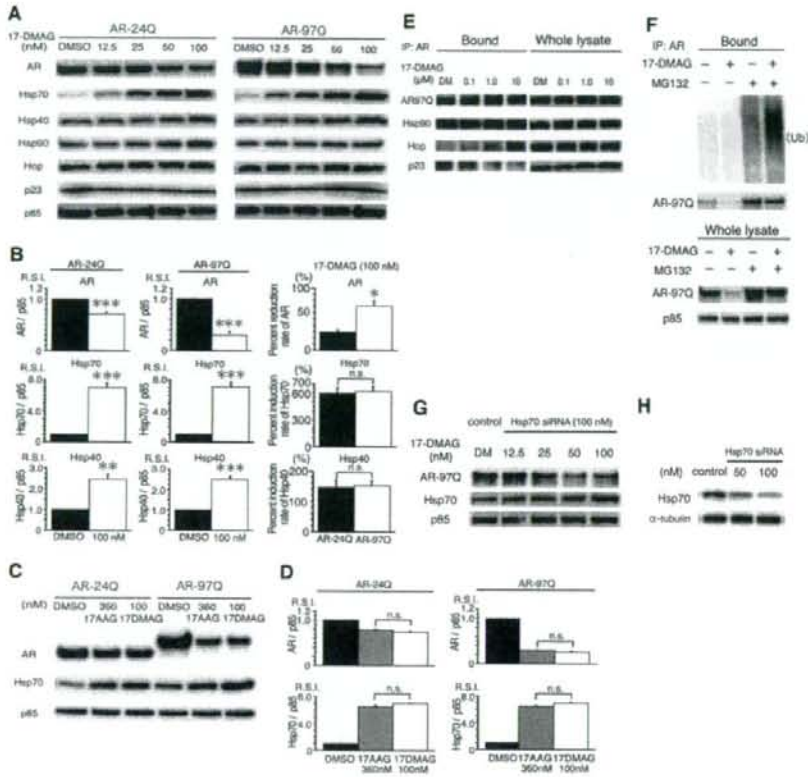

Figure 4. Effect of 17-DMAG on expression levels of AR or chaperones and on ubiquitination of AR in cultured cells. (**A**) Immunoblots of AR and chaperone proteins from transfected SH-SY5Y cells highly expressing the wild-type (AR-24Q) or mutant (AR-97Q) AR and treated with the indicated doses of 17-DMAG or with the vehicle DMSO. p85 was used as a loading control. (**B**) Densitometric analyses of AR, Hsp70 and Hsp40 in vehicle (DMSO) and 17-DMAG (100 nM) treated SH-SY5Y cells expressing the wild-type (AR-24Q) or mutant (AR-97Q) AR. Values are expressed as mean ± SE, $n = 5$; $^{*}P < 0.005$; $^{**}P < 0.0005$; $^{***}P < 0.0001$. (**C**) Western blot analysis of AR and Hsp70 proteins in SH-SY5Y cells expressing AR-24Q or AR-97Q following treatment with the indicated doses of 17-AAG, 17-DMAG or with the vehicle DMSO. (**D**) Densitometric analyses of AR and Hsp70 in vehicle (DMSO), 17-AAG (360 nM) and 17-DMAG (100 nM) treated SH-SY5Y cells expressing AR-24Q or AR-97Q. The decreases in both ARs and the induction of Hsp70 expression following 17-AAG or 17-DMAG were similar, but the concentration of 17-AAG was more than three times that of 17-DMAG. Values are expressed as mean ± SE, $n = 5$. (**E**) Pharmacological changes in the AR-Hsp90 complex. Transfected cells expressing mutant AR were treated with the indicated doses of 17-DMAG or DMSO (DM) for 30 min, immunoprecipitated with an anti-AR antibody and then immunoblotted with antibodies against the indicated Hsp90 chaperone complex proteins and client proteins. Note that the short time exposure to 17-DMAG did not decrease the amount of mutant AR. (**F**) Effect of 17-DMAG, in the presence of the proteasome inhibitor MG132, on ubiquitination and AR expression. (**G**) Immunoblot showing the effects of 17-DMAG or DMSO (DM) on the expression of mutant AR when Hsp70 induction was inhibited by siRNA. (**H**) Western blot analysis of endogenous Hsp70 protein expression from SH-SY5Y cells exposed to the control oligonucleotide or indicated concentrations of siRNA for 48 h.

17-DMAG preferentially degrades mutant AR protein and significantly increases Hsp70 and Hsp40 in SBMA mice

Treatment with 17-DMAG significantly diminished both the high-molecular-weight complex and the monomeric mutant AR in the spinal cord and muscle of AR-97Q mice ($P < 0.05$), but only slightly diminished the wild-type monomeric AR in AR-24Q mice (Fig. 6A and B). In the AR-97Q mice, monomeric AR decreased by 71% in the spinal cord and 70% in the skeletal muscle, but only by 37 and 27%, respectively, in the AR-24Q mice (Fig. 6A and B). RT–PCR in both AR-24Q and AR-97Q mice showed that the levels of AR mRNA were similar in the treated (Tg-10) and untreated (Tg-0) mice (Supplementary Material, Fig. S6), implying that the decreased protein was due to degradation and not to lower mRNA levels. We also conducted filter-trap assays (Supplementary Material) for both the large molecular weight aggregated and the soluble forms of mutant AR. Both forms of trapped AR-97Q protein were markedly reduced in the spinal cord and muscle of treated mice (Supplementary Material, Fig. S7). These observations indicate that 17-DMAG preferentially degrades not only the

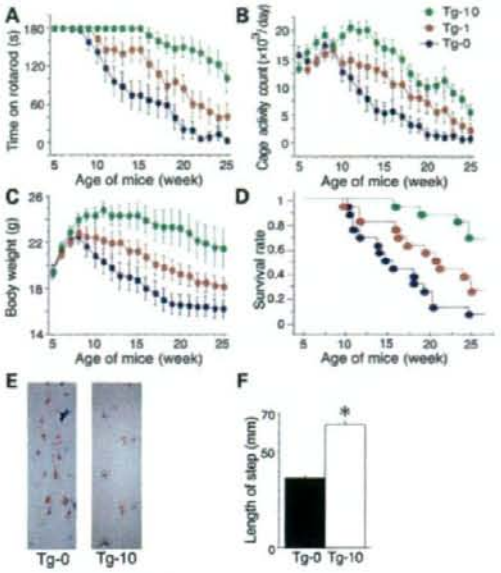

Figure 5. Effects of 17-DMAG on behavioral phenotypes in male AR-97Q mice. (**A–D**) Untreated mice (Tg-0) or those administered 1 (Tg-1) or 10 mg/kg (Tg-10) 17-DMAG from age 5 to 25 weeks were tested on the Rotarod task (A) for cage activity (B) and body weight (C). All parameters were significantly different between the Tg-0 and Tg-10 mice ($P < 0.005$ for all parameters, $n = 16$). (D) A Kaplan–Meier plot shows the prolonged survival of the Tg-1 and Tg-10 mice compared with the Tg-0 mice; $P < 0.05$; $P < 0.0001$, respectively. (**E**) Footprints of representative 16-week-old Tg-0 and Tg-10 mice. Front paws are indicated in red, and hind paws are in blue. (**F**) The length of steps was measured in 16-week-old Tg-0 and Tg-10 mice. Each column shows the average length of steps of the hind paw. Values are expressed as mean ± SE, $n = 5$; $^*P < 0.0001$.

high-molecular-weight mutant AR complex but also the monomeric mutant AR protein.

17-DMAG treatment of transgenic mice was also accompanied by marked chaperone induction. The levels of Hsp70 and Hsp40 in the spinal cord were increased by 367 ($P < 0.005$) and 105% ($P < 0.0001$), respectively, and in the muscle by 235 ($P < 0.05$) and 195% ($P < 0.0001$), respectively (Fig. 6C and D) following 17-DMAG treatment. These pharmacological effects of 17-DMAG on chaperone induction were more pronounced than those of 17-AAG in our previous study (11). The enhanced chaperone induction accompanying 17-DMAG treatment might be responsible for its enhanced pharmacological effect of reducing mutant AR.

Immunohistochemical staining for mutant AR showed a significant reduction in 1C2-positve diffuse nuclear staining and NIs in the spinal anterior horn (Fig. 6E) and skeletal muscle (Fig. 6F) in the Tg-10 mice (Fig. 6G). Anti-glial fibrillary acidic protein (GFAP) staining showed an apparent reduction in reactive astrogliosis in the Tg-10 mice in the spinal anterior horn (Fig. 6H). Muscle histology also demonstrated marked amelioration of muscle atrophy in the Tg-10 mice (Fig. 6I). AR-24Q mice and normal littermates treated with 17-DMAG displayed no altered phenotypes (data not shown).

DISCUSSION

The UPS is responsible for the turnover of most soluble proteins and plays an essential role in degrading short-lived regulatory proteins and damaged or misfolded proteins (37). We demonstrated that UPS activity during the advanced stage of SBMA model mice, assessed by chymotryptic activity and ubiquitin-dependent protein-degradation activity, was very well preserved in the spinal cord and even increased in the skeletal muscle. More importantly, the expression levels of 20S proteasome α1 and α7 subunits appeared to be elevated in the 1C2-positive muscle fibers (Supplementary Material, Fig. S4). In addition, UPS function semi-quantitatively evaluated in the GFP-based (Ub^{G76V}-GFP) reporter mouse (31) was also not impaired, data that are concordant with a previous study of an ataxia model of polyQ disease (25). Further evidence of preserved proteasomal function in the AR-97Q mice exhibiting advanced SBMA phenotypes is the data showing that protein levels of proteasome subunits in AR-97Q mice were similar to those in the AR-24Q mice in the spinal motor neurons and increased in skeletal muscle. Earlier studies of polyQ–mediated degeneration in cultured cell models (16,18,38), transgenic mice (39) and human postmortem samples (40) showed that components of the UPS are sequestrated in cellular aggregates or NIs, suggesting involvement of the UPS in polyQ diseases. The function of the UPS was evaluated in various assays that provided divergent results, ranging from impaired (19–21,24) to preserved (28,29) UPS function. It is possible that mutant polyQ-expanded proteins may directly affect proteasome function within the specific subcellular compartment of synaptic UPS activities (23), although it has been demonstrated that neuronal dysfunction can develop without significant impairment of the UPS in a mouse model of SCA7 (25). Consistent with this is data showing that proteasome impairment did not contribute to the pathogenesis of Huntington's disease in a mouse model (26). Furthermore, in conditional knockout mouse models of polyQ disease, genetic diminution of the abnormal gene led to rapid clearance of pre-existing polyQ aggregates and reversible improvement of abnormal phenotypes (41,42). If the UPS were irreversibly damaged in patients and animal models of polyQ diseases, then the aggregates of pathogenic proteins could not have been eliminated. Taking these data together, we considered that UPS function is well preserved in polyQ diseases, particularly in SBMA, and treatment with 17-DMAG, which enhances a self-clearing system of target disease-causing proteins via the UPS, is a reasonable therapeutic strategy against polyQ-related diseases. On the other hand, it is known that an age-dependent decrease in proteasome activity exists that may reduce the clearance of the misfolded proteins, resulting in their accumulation and contributing to late-onset polyQ-expanded toxicity. UPS-related genes were suppressed at the transcriptional level in the aged brain (43), and proteasome activity was also decreased in the aged brain (27,44), although brain proteasome activity was not specifically altered in the brains of Huntington's disease knock-in mice when compared with age-matched wild-type mice (27). As proteasome activity generally decreases in the central nervous system in aged animals (27,44), such an age-dependent decrease in UPS function is

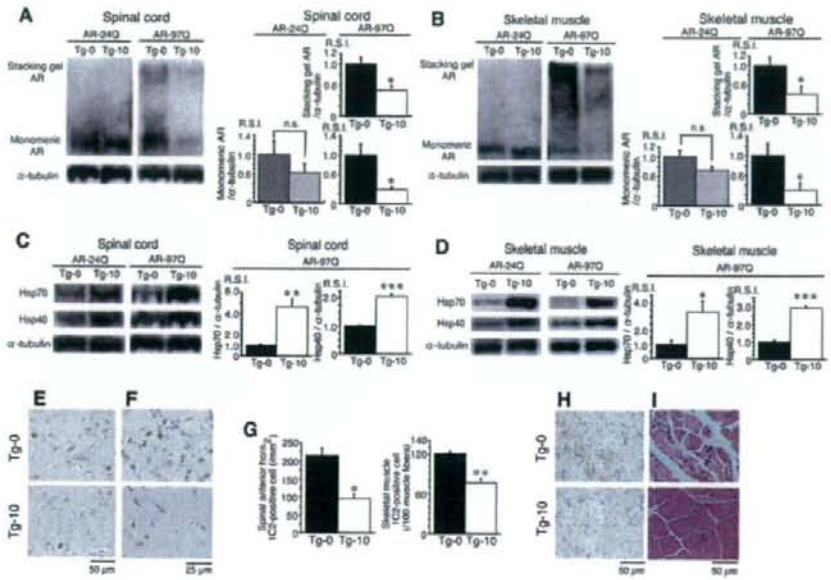

Figure 6. Effects of 17-DMAG on AR expression and histopathology in male AR-24Q and AE-97Q mice. (**A** and **B**) Western blot analyses (left) and image analysis quantification (right) of high-molecular-weight complex AR (in stacking gel) and monomeric mutant AR in the spinal cord (A) and muscle (B) of AR-24Q and AR-97Q mice probed with an AR-specific antibody. Values are expressed as mean ± SE, $n = 5$; $^{*}P < 0.05$. (**C** and **D**) Western blot analyses (left) and image analysis quantification (right) in the spinal cord (C) and muscle (D) of AR-24Q and AR-97Q mice probed with antibodies specific for the expression levels of Hsp70 and Hsp40. Values are expressed as mean ± SE, n=5. Statistical differences are indicated by asterisks; $^{*}P < 0.05$; $^{**}P < 0.005$; $^{***}P < 0.0001$. (**E** and **F**) Effects of 17-DMAG on the histopathology of male AR-97Q mice. Immunohistochemical staining with the 1C2 antibody, specific for mutant AR, showed marked differences in diffuse nuclear staining and NIs between Tg-0 and Tg-10 mice in the spinal anterior horn (E) and skeletal muscle (F). (**G**) Quantification of the number of 1C2-positive cells in the spinal cord and skeletal muscle in Tg-0 and Tg-10 mice. Values are expressed as mean ± SE, $n = 5$; $^{*}P < 0.005$; $^{**}P < 0.0005$. (**H**) Immunohistochemical staining with a GFAP-specific antibody shows reactive astrogliosis in the spinal anterior horn of untreated (Tg-0) mice and those treated with 17-DMAG. (**I**) Hematoxylin and eosin staining of the skeletal muscle in Tg-0 mice shows obvious grouped atrophy and small angulated fibers, not seen in Tg-10 mice.

unlikely to critically contribute to the region-specific neuropathology seen in different types of polyQ diseases.

We present a potent strategy for SBMA therapy, with 17-DMAG acting via a preserved or elevated proteasome activity. 17-DMAG has two major activities, preferential client protein degradation and Hsp induction; the present study revealed that polyQ-expanded mutant AR was preferentially degraded by treatment with 17-DMAG. Mutant AR elimination was mediated through its preferential incorporation into the Hsp90-chaperone complex (11,45), where it is prone to proteasomal degradation. Our present results in a transgenic mouse model also confirmed that 17-DMAG passes through the blood-brain barrier as previously reported (46) and that it demonstrates sufficient pharmacological effects in the central nervous system. We have already examined the effectiveness of 17-AAG in a mouse model of SBMA (11). 17-AAG has less toxicity (47) and higher selectivity (45) for client oncoproteins than does geldanamycin (48). 17-DMAG has a potential advantage over 17-AAG because its aqueous solubility eliminates the need for complicated formulations used to administer 17-AAG, and 17-DMAG induced the up-regulation of Hsp70 more than 17-AAG did (49). In a mouse study, the bioavailability of 17-DMAG by oral administration was twice that of orally delivered 17-AAG (46). Data from preclinical toxicity studies for 17-DMAG in animal models have recently become available (50) and phase I clinical trials for cancer are currently being performed (51,52). In addition, 17-DMAG is not metabolized to the potentially toxic metabolites that arise from CYP3A-mediated metabolism of the 17-allyl side chain of 17-AAG (14,46,53), indicating that 17-DMAG has less toxic side effects than 17-AAG. In fact, 17-DMAG shows greater oral bioavailability than 17-AAG, the pharmacological effect of 17-DMAG for mutant AR degradation was three times that of 17-AAG (Fig. 4C and D), and the inductions of Hsp70 and Hsp40 with 17-DMAG were more pronounced than with 17-AAG in the SBMA mouse model (Fig. 6C and D) (11). Moreover, the concentration necessary to obtain a similar therapeutic efficacy using 17-DMAG (10 mg/kg) was much lower than that using 17-AAG (25 mg/kg) (Fig. 5A–D) (11). Although 17-DMAG passes through the blood-brain barrier less than 17-AAG *in vivo* (14,46), these data show that 17-DMAG has more potent effects than 17-AAG.

Hsp90 inhibitors also function as Hsp inducers (54,55), resulting in the dissociation of HSF-1 from the Hsp90 complex and subsequent HSF-1 trimerization, thereby leading to Hsp activation (11). In this study, the inductions of Hsp70 and Hsp40 with 17-DMAG were more pronounced than with

17-AAG in our previous study (11). Hsps, particularly Hsp70, were shown to suppress aggregate formation and cellular toxicity in polyQ disease models (9,16,56). Hsp70 over-expression also enhanced degradation of polyQ-expanded proteins via its interaction with the UPS (36,57). CHIP (carboxyl terminus of Hsc70-interacting protein) might be one such coupling factor between the Hsp70 chaperone system and the machinery responsible for degrading mutant proteins (58,59). Thus, enhancement of chaperone expression using Hsp90 inhibitors under preserved UPS function is a further reasonable clinical approach for the treatment of pathogenic mutant or modified protein-mediated neurodegenerative diseases.

In conclusion, we have demonstrated that UPS function was well preserved or even enhanced in an SBMA model mouse and that 17-DMAG exerted potent therapeutic effects on the SBMA phenotype. In the case of other neurodegenerative diseases, phosphorylated tau would be one of the target proteins of Hsp90 inhibitors (60). Hsp90 inhibitors have also been shown to be effective in animal models of Parkinson's disease (61), stroke (62) and autoimmune encephalomyelitis (63). The combined therapy of 17-DMAG and leuprorelin would be expected to be more effective than the monotherapy with either 17-DMAG or leuprorelin (64), because the target sites of the agents are different and thus the therapeutic effect of the combined therapy would theoretically be additive or synergistic. 17-DMAG, by directly reducing disease-causing protein, presents a new therapeutic avenue for SBMA and has potentially widespread applications for other neurodegenerative diseases, particularly if the disease-causing protein belongs to the Hsp90 client protein family.

MATERIALS AND METHODS

DNA transfection

Full-length *AR* cDNAs were constructed by subcloning *AR* inserts into the pCR3.1 mammalian expression vector (Invitrogen) (11). SH-SY5Y cells were plated in 6 cm dishes in 5 ml of DMEM/F12 containing 10% fetal bovine serum with penicillin and streptomycin, and each dish was transfected with 8 μg of vector containing AR24, AR97 or mock (negative control) constructs using OPTI-MEM (Invitrogen) and Lipofectamine 2000 (Invitrogen) according to the manufacturer's instructions. The cells were cultured for 48 h at 37°C under 5% CO_2. Transfection efficiency was 60–70% in both AR-24Q and AR-97Q transfected cells, and no difference in transfection efficiencies was found. In this culture system, we detected a band of monomeric mutant AR in the separating gel, but barely detected the high-molecular-weight mutant AR protein complex, which was retained in the stacking gel. Therefore, this cultured cell model is better suited for estimating changes in monomeric mutant AR expression.

Therapeutic agents and protocol for administration

17-DMAG (NSC707545) was obtained from the Regulatory Affairs Branch, Division of Cancer Treatment and Diagnosis, National Cancer Institute (Bethesda, MD, USA) and Kosan Biosciences (Hayward, CA, USA). For cultured cell models, a 1 mM stock solution of 17-DMAG in DMSO was diluted into fresh medium to give final concentrations of 12.5–100 nM and added to the washed cells 24 h after transfection. Control cells were treated with DMSO alone. To show obvious pharmacological changes in the AR-Hsp90 complex, as demonstrated in a previous report (11), we exposed cultured cells to 17-DMAG for 30 min at concentrations of 0.1, 1.0 and 10 μM, 48 h after transfection.

For transgenic mice, the dosing solutions of 17-DMAG in saline were freshly prepared weekly. 17-DMAG treatments were started when mice were 5 weeks old and were continued until they were 16 weeks (or 25 weeks for toxicity studies). An optimal dose of 17-DMAG was determined based on a previous study in mice (50). Male AR-24Q and AR-97Q mice received 0.2 ml oral administration of 1 or 10 mg/kg 17-DMAG three times a week on alternate days; control mice received saline alone. Members of the same litter were distributed among the three treatment groups and homogeneities of body weight variances and means among the three groups were confirmed using Bartlett's test and one-way ANOVA.

Assay of proteasome activity

Mouse tissue homogenates from the spinal cord and muscle of 16-week-old AR-24Q and AR-97Q mice were clarified by centrifugation at 15 000 *g* and subjected to 8–32% (v/v) linear glycerol density gradient centrifugation (22 h, 83 000*g*). Proteasome chymotrypsin-like peptidase activity was measured using the peptide substrate, succinyl-Leu-Leu-Val-Tyr-7-amino-4-methyl-coumarin in the absence (i.e. 26S proteasome) of 0.025% sodium dodecyl sulfate (SDS) as described previously (65). For the assay of cIAP1 (inhibitor of apoptosis-1) degradation, cDNAs encoding Flag-cIAP1 subcloned into pcDNA3.1 were transcribed *in vitro*, translated and radiolabeled. The 35S-labeled Flag-cIAP1 was purified using M2-agarose (Sigma) and eluted with Flag-peptide (Sigma). The results were confirmed by duplicate measurements of the samples from different mice. For ubiquitination of cIAP1, 3 000 000 c.p.m. of 35S-labeled cIAP1, 0.25 μg of E1, 0.9 μg of UbcH5 and 33 μg of ubiquitin (Sigma) were mixed and incubated in a volume of 80 μl for 90 min at 30°C, as described previously (66). Finally, 2.5 ml of the ubiquitination mixture was added to 10 μl of cell lysate in the presence of 2 mM ATP, incubated at 37°C for 20 min and then radioactivities of trichloroacetic acid-soluble fractions were measured.

Generation and maintenance of TG mice and genotyping

We crossed the mice expressing full-length human AR with 24- (AR-24Q mice, 5-5 line) or 97-polyQ tracts (AR-97Q mice, 7-8 line) with Ub^{G76V}-GFP/1 line. The Ub^{G76V}-GFP/1 line was obtained from Dr Nico P. Dantuma in the Department of Cell and Molecular Biology, Karolinska Institute, and maintained in the B6 background. We screened mouse-tail DNA by PCR for the presence of the transgene using the primer sets as described previously (30,31).

Neurological and behavioral assessment of SBMA model mice

The AR-24Q and AR-97Q mice were generated and maintained as previously described (67). The AR-97Q male mice showed

progressive muscular atrophy and weakness as well as diffuse nuclear staining and NIs consisting of mutant AR. These phenotypes were very pronounced in male transgenic mice similar to SBMA patients (30). All animal experiments were performed in accordance with the National Institutes of Health Guide for the Care and Use of Laboratory Animals and under the approval of the Nagoya University Animal Experiment Committee. The mouse Rotarod task was performed using an Economex Rotarod (Ugo Basile), and cage activity was measured with the AB system (BrainScience Idea Osaka, Japan) as described previously (30,68). The investigators in the behavioral assessment were blinded to the treatments.

Protein expression analysis

Cells were lysed in CelLytic-M Mammalian Cell Lysis/Extraction Reagent (Sigma) with 1 mM PMSF and 6 μg/ml aprotinine and centrifuged at 15 000*g* for 15 min at 4°C, 48 h after transfection. Sixteen-week-old mice were exsanguinated under ketamine–xylazine anesthesia 12 h after the final treatment of 17-DMAG, and tissues were snap-frozen with powdered CO_2 in acetone. The tissues were homogenized in CelLytic-M Mammalian Cell Lysis/Extraction Reagent (Sigma) with 1 mM PMSF and 6 μg/ml aprotinine and centrifuged at 2500*g* for 15 min at 4°C. Supernatant fraction protein concentrations were determined using the DC protein assay (Bio-Rad). Aliquots of supernatant fractions were loaded on 5–20% SDS–PAGE gels, each lane containing 7 μg protein for cells, 160 μg for nervous tissue and 80 μg for muscular tissue, and then transferred to Hybond-P membranes (GE Healthcare) using 25 mM Tris, 192 mM glycine, 0.1% SDS and 10% methanol as transfer buffer. Primary antibodies were used at the following concentrations: rabbit anti-AR (1:1000, H280; Santa Cruz or 1:1000, N-20; Santa Cruz); mouse anti-Hsp70 (1:1000, SPA-810; Assay Designs); rabbit anti-Hsp40 (1:5000, SPA-400; Assay Designs); mouse anti-Hsp90 (1:1000, F-8; Santa Cruz); mouse anti-Hop (1:1000, SRA-1500; Assay Designs); mouse anti-p23 (1:1000, MA3-414; Affinity BioReagents); rabbit anti-p85 (1:2000, Upstate); and mouse anti-α-tubulin (1:5000, T9026; Sigma); mouse anti-GFP (1:5000, MAB3580; Millipore); anti-20S proteasome subunits α3, α4, α5 and α6 (Biomol); anti-20S proteasome subunits β2, β3, β4, β5i, β6 and β7 (Biomol); anti-19S proteasome subunits Rpt1, Rpt2, Rpt3, Rpt4, Rpt5 and Rpt6 (Biomol); rabbit anti-11S proteasome regulator (PA28) PA28α, PA28β, PA28γ subunits (Biomol); rabbit anti-20S proteasome α1, α2, α7, β1; mouse anti-19S proteasome subunit Rpn2; and rabbit anti-19S proteasome subunits Rpn1, Rpn7, Rpn8 (1:1000) (65,69,70). Primary antibodies were probed using HRP-conjugated anti-rabbit Ig F $(ab')_2$ and anti-mouse Ig F $(ab')_2$ (1:5000, GE Healthcare) secondary antibodies and detected with the ECL+plus kit (GE Healthcare). An LAS-3000 imaging system was used to produce digital images and to quantify band intensities, which were then analyzed with Image Gauge software version 4.22 (Fujifilm, Tokyo, Japan). Densitometric values of AR, Hsp70, Hsp40 and GFP were normalized to those of endogenous p85 or α-tubulin. Relative signal intensity (RSI) was computed as the signal intensity of each sample divided by that of the Tg-0 mice (Fig. 6) or the 24Q/GFP mice (Fig. 2).

Immunoprecipitation from cultured cells was performed using 300 μg total protein lysate from cells, 10 μl Protein G Sepharose (GE Healthcare) and 5 μl anti-AR antibody (N-20; Santa Cruz). For experiments involving co-precipitation of AR, cells were lysed in molybdate-containing lysis buffer (10 mM Tris pH 7.4, 10 mM monothioglycerol, 10 mM Na_2MoO_4, 10 mM $MgCl_2$, 0.2% Tween-20, 1 mM PMSF and 6 μg/ml aprotinine). For the AR ubiquitination assay, a full-length AR was constructed by subcloning AR inserts derived from pCR-AR97 (97 CAG repeats) into the pDsRed monomer mammalian expression vector (Takara Bio, Otsu, Japan) (59). SH-SY5Y cells were seeded onto 60-mm plates and transfected with plasmids encoding DsRed-AR97 for a 48 h period. Cells were exposed to MG132 (20 μM) for a 1 h period and to MG132 (20 μM) and 17-DMAG (10 μM) for a 4 h period. Extracts were prepared and AR was immunoprecipitated with anti-DsRed antibody. Blots were probed with ubiquitin (1B3; MBL) and AR (N20; Santa Cruz) antibody.

Filter-trap assay

To quantify the large-molecular aggregated and soluble form of the mutant AR protein, filter-trap assays of total tissue homogenates from the spinal cord and muscle of male AR-24Q or AR-97Q mice (16 weeks old) were performed as previously described (36). Filtration of proteins through a 0.2 μm cellulose acetate membrane (Sartorius AG) was performed using a slot-blot apparatus (Bio-Rad). Only the larger-sized mutant AR protein was retained on the cellulose acetate membrane (pore 0.2 μm in diameter), whereas the nitrocellulose membrane captured protein of all sizes. In each case, the nitrocellulose membrane was placed under the cellulose acetate membrane to capture the soluble AR protein passing through this membrane. The membranes, supported by two pieces of filter paper (Bio-Rad), were washed three times with TBS buffer. Samples of protein, 200 μg for the spinal cord and 80 μg for the muscle, were prepared in a final volume of 200 μl lysis buffer, loaded and gently vacuumed. Membranes were washed three times with TBS containing 0.05% Tween-20. Slot-blots were probed as described for western blots by an antibody against AR (H-280; Santa Cruz) or α-tubulin (T9026; Sigma).

Quantitative real-time RT–PCR

The levels of AR and proteasomal subunit mRNAs were determined by real-time RT–PCR as described previously (11). Total RNA was isolated from SH-SY5Y cells using the RNeasy Mini Kit (QIAGEN) and from transgenic mouse spinal cord and muscle by homogenizing in Trizol (Invitrogen) according to the manufacturer's instructions. Total RNA (5 μg) from cells and mouse spinal cord and muscle were reverse transcribed using SuperScript III reverse transcriptase (Invitrogen). PCR primers were designed to amplify GFP cDNA sequences in GFP-reporter mouse tissues (5′-TATAT CATGGCCGACAAGCA and 5′-TGTTCTGCTGGTAGT GGTCG) (Fig. 2), proteasomal subunit cDNA sequences in mouse tissues (Psm a3: QT00168728, Psm a5: QT00137928, Psm a6: QT00124439, Psm b1: QT00121079, Psm b5: QT 00111216, Psm c5: QT00162022 and Psm e3: QT00167797)

(QIAGEN) (Supplementary Material, Fig. S3) and AR cDNA sequences in mouse tissues (5′-TTCCACACCCAGTGAAG C-3 and 5′-CCTGAGGAGTGAATTGATCC-3′) (Supplementary Material, Fig. S5). Real-time RT–PCR was carried out in a total volume of 50 μl, containing 25 μl of 2× QuantiTect SYBR Green PCR Master Mix (QIAGEN) and 10 μM of each primer. PCR products were detected by the iCycler system (Bio-Rad). The reaction conditions were 95°C for 15 min and then 45 cycles of 15 s at 94°C, 30 s at 55°C and 30 s at 72°C. As an internal standard control, the expression level of glyceraldehyde-3-phosphate dehydrogenase (GAPDH) was simultaneously quantified using the primers (5′-CTCAGAGGAG CCCAGATGA-3′ and 5′-GCTGGTCTTGCGGTACAGT-3′) for mouse tissues. RSI was computed as the signal intensity of each sample divided by that of the AR-24Q/GFP mice (Fig. 2), the AR-24Q mice (Supplementary Material, Fig. S3) or the Tg-0 mice (Supplementary Material, Fig. S5).

RNA interference

Oligonucleotide siRNA duplexes were synthesized by Takara Bio. siRNA sequences were as follows: scramble (control) siRNA, 5′-CAAUACUGAAGUAUCAACG-3′; Hsp70 siRNA, 5′-CGAAAGACAACAAUCUGUU-3′. Transfection was done using Lipofectamine 2000 (Invitrogen) according to the manufacturer's instructions. Hsp70 was efficiently downregulated upon siRNA exposure (Fig. 4H).

Cell viability assay

MTS-based cell proliferation assays were performed in triplicate using the CellTiter 96® AQueous One Solution Cell Proliferation Assay (Promega) 48 h after incubation with 17-DMAG.

Immunohistochemistry and histopathology

Mice were deeply anesthetized with ketamine–xylazine and transcardially perfused with 20 ml of 4% paraformaldehyde fixative in phosphate buffer (pH 7.4). Tissues were post-fixed overnight in 10% phosphate-buffered formalin and processed for paraffin embedding. At room temperature, 6 μm thick tissue sections were deparaffinized, dehydrated with alcohol and treated with formic acid for 5 min. The tissue sections were blocked with normal horse serum (1:20) and incubated with mouse anti-expanded polyQ antibody (1:10 000, 1C2; Millipore); mouse anti-GFAP antibody (1:1000, Boehringer Manheim Biochemica, Manheim, Germany); anti-20S proteasome subunits α4, α5, β2; anti-19S proteasome subunit Rpt3 (Biomol); and rabbit anti-20S proteasome α1 and α7. Primary antibodies were probed with a biotinylated anti-species specific IgG secondary antibodies (Vector Laboratories) and the immune complexes visualized using streptavidin-horseradish peroxidase (Dako) and 3,3′-diaminobenzidine as a substrate. Sections were counterstained with Mayer's hematoxylin. Paraffin-embedded, 6 μm thick sections of the gastrocnemius muscles were air-dried and stained with hematoxylin and eosin. Tissues from the GFP-reporter mice were post-fixed in 4% PFA in PBS (pH 7.4) for 16 h at 4°C. The tissues were immersed in a graded series of sucrose solutions in 0.01 M PBS at 4°C as follows: 3 h in 7% sucrose, 3 h in 14% sucrose and 16 h in 25% sucrose. The tissues were then embedded in Tissue-Tek OCT compound (Sakura Finetek) and frozen with powdered solid CO_2 in acetone (71). Because native GFP fluorescence was below the detection threshold in both the spinal cord and skeletal muscle, the expression of Ub^{G76V}-GFP was evaluated semi-quantitatively by immunohistochemistry with an anti-GFP antibody. Cryostat sections, 10 μm thick, were prepared from the frozen tissues and blocked with 5% goat serum, incubated with rabbit anti-GFP antibody (1:1000, NB600-308; Novus Biologicals) at 4°C overnight, and then incubated with Alexa 488-conjugated goat anti-rabbit IgG (1:1000; Invitrogen) at 4°C overnight. The stained sections were examined and photographed with a confocal laser scanning microscope (LSM 5 PASCAL; Carl Zeiss). To assess GFP-reporter expression levels in spinal anterior horn cells, immunohistochemistry signal intensities were quantified in at least 10 transverse sections from each mouse. Images of individual anterior horn cells on transverse sections of the spinal cord with signals for Ub^{G76V}-GFP reporter were captured at the desired magnification and stored with image software (Olympus, Tokyo, Japan). Levels of reporter in the images were quantitatively analyzed with image analysis software (WinROOF version 5, Mitani, Fukui, Japan). Signal intensities were expressed as individual intracellular signal levels of Ub^{G76V}-GFP reporter (arbitrary absorbance units) in spinal anterior horn cells by subtracting the mean background levels of three regions of interest in each section. For double-immunofluorescence staining of the spinal cord and skeletal muscle, sections were blocked with 5% normal goat serum and then sequentially incubated with anti-20S proteasome α1 or α7 subunit (1:200) and 1C2 antibody (1:10 000) at 4°C overnight. The sections were then incubated with Alexa 488-conjugated goat anti-rabbit IgG (1:1000; Molecular Probes) and Alexa 568-conjugated goat anti-mouse IgG (1:1000; Molecular Probes) for 8 h at 4°C. The stained sections were examined and photographed with a confocal laser scanning microscope (LSM 5 PASCAL; Carl Zeiss MicroImaging, Tokyo, Japan).

In situ hybridization

Formalin-fixed, paraffin-embedded 6 μm thick sections of spinal cord and skeletal muscle were processed for *in situ* hybridization using the Ventana Discovery system (Ventana) according to the manufacturer's instructions. GFP cDNA was obtained using the primers 5′-CCTGAAGTTCATCTGC ACCA-3′ and 5′- GTTCACCTTGATGCCGTTCT-3′. Digoxigenin-labeled cRNA antisense and sense probes of ~350 bp were generated for *in situ* hybridization from linearized plasmids for Ub^{G76V}-GFP reporter using Sp6 and T7 polymerases (Roche), respectively. No hybridization signal was observed with the sense probe for the expression of Ub^{G76V}-GFP reporter (data not shown). To assess gene expression levels in spinal anterior horn cells, signal intensities of *in situ* hybridization were quantified in at least 10 transverse sections from each mouse. Images of individual anterior horn cells on transverse sections of the spinal cord with signals for Ub^{G76V}-GFP reporter were captured at the desired magnification and stored with image software (Olympus). Signal levels of the images were

quantitatively analyzed with image analysis software (WinRoof version 5) and expressed as individual intracellular cytoplasmic signal levels (arbitrary absorbance units) of spinal anterior horn cells for Ub^{G76V}-GFP reporter by subtracting the mean background levels of three regions of interest in each section.

Quantification of 1C2-positive cells, glial cell reaction and muscle fiber size

For assessment of 1C2-positive cells, 6 μm thick coronal sections of the thoracic spinal cord and gastrocnemius muscle stained with 1C2 antibody (1:10 000, Millipore) were prepared and the number of 1C2-positive cells in each individual mouse was counted using a light microscope with a computer-assisted image analyzer (Luzex FS, Nikon, Tokyo, Japan). For assessment of 1C2-positive cells in the ventral horn of the spinal cord, 50 consecutive transverse sections of the thoracic spinal cord were prepared and 1C2-positive cells within the ventral horn of every fifth section were counted as described previously (64). Populations of 1C2-positive cells were expressed as the number per mm^2. For assessment of 1C2-positive cells in muscle, the number of 1C2-positive cells was calculated from counts of more than 500 fibers in randomly selected areas and expressed as the number per 100 muscle fibers. The quantitative data of six individual mice were expressed as mean ± SE.

Hematological examination

AST and ALT were measured by ultraviolet spectrophotometry, BUN by the Urease-GLDH UV assay and Cre by an enzyme assay (Mitsubishi Kagaku Bio-Clinical Laboratories, Tokyo, Japan).

Statistical analyses

Data were analyzed by unpaired *t*-tests in Figures 1B, 2, 4B, 4D, 5F and 6 and Supplementary Material, Figures S1, S3, S5 and S6 and Kaplan–Meier and log-rank tests for survival rate in Figure 5D using Statview software version 5 (HULINKS, Tokyo, Japan). Statistical significance of the drug–dose dependency of phenotypes in Figure 5A–C was examined by the Williams test for multiple comparisons using Microsoft Excel 2004 (Microsoft).

SUPPLEMENTARY MATERIAL

Supplementary Material is available at *HMG* online.

ACKNOWLEDGEMENTS

We thank the National Cancer Institute and Kosan Biosciences for kindly providing 17-DMAG, and Noboru Ogiso, Yasutaka Ohya and Kumiko Yano in the Division for Research of Laboratory Animals, Center for Research of Laboratory Animals and Medical Research Engineering for their technical assistances. We also thank Dr Nico P. Dantuma for kindly providing the Ub^{G76V}-GFP reporter mice.

Conflict of Interest statement. None declared.

FUNDING

This work was supported by a Center-of-Excellence (COE) grant and Grant-in-Aid for Scientific Research on Priority Areas (Research on Pathomechanisms of Brain Disorders) from Ministry of Education, Culture, Sports, Science and Technology of Japan and by Health and Labour Sciences Research Grants for research on psychiatric and neurological diseases and mental health from Ministry of Health, Labour and Welfare of Japan.

REFERENCES

1. Di Prospero, N.A. and Fischbeck, K.H. (2005) Therapeutics development for triplet repeat expansion diseases. *Nat. Rev. Genet.*, **6**, 756–765.
2. Adachi, H., Waza, M., Katsuno, M., Tanaka, F., Doyu, M. and Sobue, G. (2007) Pathogenesis and molecular targeted therapy of spinal and bulbar muscular atrophy. *Neuropathol. Appl. Neurobiol.*, **33**, 135–151.
3. Tanaka, F., Doyu, M., Ito, Y., Matsumoto, M., Mitsuma, T., Abe, K., Aoki, M., Itoyama, Y., Fischbeck, K.H. and Sobue, G. (1996) Founder effect in spinal and bulbar muscular atrophy (SBMA). *Hum. Mol. Genet.*, **5**, 1253–1257.
4. Sobue, G., Hashizume, Y., Mukai, E., Hirayama, M., Mitsuma, T. and Takahashi, A. (1989) X-linked recessive bulbospinal neuronopathy. A clinicopathological study. *Brain.* **112** (Pt 1), 209–232.
5. Adachi, H., Katsuno, M., Minamiyama, M., Waza, M., Sang, C., Nakagomi, Y., Kobayashi, Y., Tanaka, F., Doyu, M., Inukai, A. *et al.* (2005) Widespread nuclear and cytoplasmic accumulation of mutant androgen receptor in SBMA patients. *Brain*, **128**, 659–670.
6. Pratt, W.B. and Toft, D.O. (2003) Regulation of signaling protein function and trafficking by the hsp90/hsp70-based chaperone machinery. *Exp. Biol. Med. (Maywood)*, **228**, 111–133.
7. Poletti, A. (2004) The polyglutamine tract of androgen receptor: from functions to dysfunctions in motor neurons. *Front. Neuroendocrinol.*, **25**, 1–26.
8. Neckers, L. (2002) Heat shock protein 90 inhibition by 17-allylamino-17-demethoxygeldanamycin: a novel therapeutic approach for treating hormone-refractory prostate cancer. *Clin. Cancer Res.*, **8**, 962–966.
9. Muchowski, P.J. and Wacker, J.L. (2005) Modulation of neurodegeneration by molecular chaperones. *Nat. Rev. Neurosci.*, **6**, 11–22.
10. Workman, P., Burrows, F., Neckers, L. and Rosen, N. (2007) Drugging the cancer chaperone HSP90: combinatorial therapeutic exploitation of oncogene addiction and tumor stress. *Ann. N. Y. Acad. Sci.*, **1113**, 202–216.
11. Waza, M., Adachi, H., Katsuno, M., Minamiyama, M., Sang, C., Tanaka, F., Inukai, A., Doyu, M. and Sobue, G. (2005) 17-AAG, an Hsp90 inhibitor, ameliorates polyglutamine-mediated motor neuron degeneration. *Nat. Med.*, **11**, 1088–1095.
12. Smith, V., Sausville, E.A., Camalier, R.F., Fiebig, H.H. and Burger, A.M. (2005) Comparison of 17-dimethylaminoethylamino-17-demethoxy-geldanamycin (17DMAG) and 17-allylamino-17-demethoxygeldanamycin (17AAG) in vitro: effects on Hsp90 and client proteins in melanoma models. *Cancer Chemother. Pharmacol.*, **56**, 126–137.
13. Herbst, M. and Wanker, E.E. (2007) Small molecule inducers of heat-shock response reduce polyQ-mediated huntingtin aggregation. A possible therapeutic strategy. *Neurodegener. Dis.*, **4**, 254–260.
14. Egorin, M.J., Lagattuta, T.F., Hamburger, D.R., Covey, J.M., White, K.D., Musser, S.M. and Eiseman, J.L. (2002) Pharmacokinetics, tissue distribution, and metabolism of 17-(dimethylaminoethylamino)-17-demethoxygeldanamycin (NSC 707545) in CD2F1 mice and Fischer 344 rats. *Cancer Chemother. Pharmacol.*, **49**, 7–19.
15. La Spada, A.R. and Weydt, P. (2005) Targeting toxic proteins for turnover. *Nat. Med.*, **11**, 1052–1053.
16. Cummings, C.J., Mancini, M.A., Antalffy, B., DeFranco, D.B., Orr, H.T. and Zoghbi, H.Y. (1998) Chaperone suppression of aggregation and altered subcellular proteasome localization imply protein misfolding in SCA1. *Nat. Genet.*, **19**, 148–154.

17. Ciechanover, A. and Brundin, P. (2003) The ubiquitin proteasome system in neurodegenerative diseases: sometimes the chicken, sometimes the egg. *Neuron*, **40**, 427–446.
18. Bence, N.F., Sampat, R.M. and Kopito, R.R. (2001) Impairment of the ubiquitin-proteasome system by protein aggregation. *Science*, **292**, 1552–1555.
19. Jana, N.R., Zemskov, E.A., Wang, G. and Nukina, N. (2001) Altered proteasomal function due to the expression of polyglutamine-expanded truncated N-terminal huntingtin induces apoptosis by caspase activation through mitochondrial cytochrome c release. *Hum. Mol. Genet.*, **10**, 1049–1059.
20. Bennett, E.J., Bence, N.F., Jayakumar, R. and Kopito, R.R. (2005) Global impairment of the ubiquitin-proteasome system by nuclear or cytoplasmic protein aggregates precedes inclusion body formation. *Mol. Cell*, **17**, 351–365.
21. Bennett, E.J., Shaler, T.A., Woodman, B., Ryu, K.Y., Zaitseva, T.S., Becker, C.H., Bates, G.P., Schulman, H. and Kopito, R.R. (2007) Global changes to the ubiquitin system in Huntington's disease. *Nature*, **448**, 704–708.
22. Rusmini, P., Sau, D., Crippa, V., Palazzolo, I., Simonini, F., Onesto, E., Martini, L. and Poletti, A. (2007) Aggregation and proteasome: the case of elongated polyglutamine aggregation in spinal and bulbar muscular atrophy. *Neurobiol. Aging*, **28**, 1099–1111.
23. Wang, J., Wang, C.E., Orr, A., Tydlacka, S., Li, S.H. and Li, X.J. (2008) Impaired ubiquitin-proteasome system activity in the synapses of Huntington's disease mice. *J. Cell Biol.*, **180**, 1177–1189.
24. Seo, H., Sonntag, K.C. and Isacson, O. (2004) Generalized brain and skin proteasome inhibition in Huntington's disease. *Ann. Neurol.*, **56**, 319–328.
25. Bowman, A.B., Yoo, S.Y., Dantuma, N.P. and Zoghbi, H.Y. (2005) Neuronal dysfunction in a polyglutamine disease model occurs in the absence of ubiquitin-proteasome system impairment and inversely correlates with the degree of nuclear inclusion formation. *Hum. Mol. Genet.*, **14**, 679–691.
26. Bett, J.S., Goellner, G.M., Woodman, B., Pratt, G., Rechsteiner, M. and Bates, G.P. (2006) Proteasome impairment does not contribute to pathogenesis in R6/2 Huntington's disease mice: exclusion of proteasome activator REGgamma as a therapeutic target. *Hum. Mol. Genet.*, **15**, 33–44.
27. Zhou, H., Cao, F., Wang, Z., Yu, Z.X., Nguyen, H.P., Evans, J., Li, S.H. and Li, X.J. (2003) Huntingtin forms toxic NH2-terminal fragment complexes that are promoted by the age-dependent decrease in proteasome activity. *J. Cell Biol.*, **163**, 109–118.
28. Ding, Q., Lewis, J.J., Strum, K.M., Dimayuga, E., Bruce-Keller, A.J., Dunn, J.C. and Keller, J.N. (2002) Polyglutamine expansion, protein aggregation, proteasome activity, and neural survival. *J. Biol. Chem.*, **277**, 13935–13942.
29. Diaz-Hernandez, M., Hernandez, F., Martin-Aparicio, E., Gomez-Ramos, P., Moran, M.A., Castano, J.G., Ferrer, I., Avila, J. and Lucas, J.J. (2003) Neuronal induction of the immunoproteasome in Huntington's disease. *J. Neurosci.*, **23**, 11653–11661.
30. Katsuno, M., Adachi, H., Kume, A., Li, M., Nakagomi, Y., Niwa, H., Sang, C., Kobayashi, Y., Doyu, M. and Sobue, G. (2002) Testosterone reduction prevents phenotypic expression in a transgenic mouse model of spinal and bulbar muscular atrophy. *Neuron*, **35**, 843–854.
31. Lindsten, K., Menendez-Benito, V., Masucci, M.G. and Dantuma, N.P. (2003) A transgenic mouse model of the ubiquitin/proteasome system. *Nat. Biotechnol.*, **21**, 897–902.
32. Dantuma, N.P., Lindsten, K., Glas, R., Jellne, M. and Masucci, M.G. (2000) Short-lived green fluorescent proteins for quantifying ubiquitin/proteasome-dependent proteolysis in living cells. *Nat. Biotechnol.*, **18**, 538–543.
33. Whitesell, L. and Cook, P. (1996) Stable and specific binding of heat shock protein 90 by geldanamycin disrupts glucocorticoid receptor function in intact cells. *Mol. Endocrinol.*, **10**, 705–712.
34. Mimnaugh, E.G., Chavany, C. and Neckers, L. (1996) Polyubiquitination and proteasomal degradation of the p185c-erbB-2 receptor protein-tyrosine kinase induced by geldanamycin. *J. Biol. Chem.*, **271**, 22796–22801.
35. Bonvini, P., Dalla Rosa, H., Vignes, N. and Rosolen, A. (2004) Ubiquitination and proteasomal degradation of nucleophosmin-anaplastic lymphoma kinase induced by 17-allylamino-demethoxygeldanamycin: role of the co-chaperone carboxyl heat shock protein 70-interacting protein. *Cancer Res.*, **64**, 3256–3264.
36. Adachi, H., Katsuno, M., Minamiyama, M., Sang, C., Pagoulatos, G., Angelidis, C., Kusakabe, M., Yoshiki, A., Kobayashi, Y., Doyu, M. *et al.* (2003) Heat shock protein 70 chaperone overexpression ameliorates phenotypes of the spinal and bulbar muscular atrophy transgenic mouse model by reducing nuclear-localized mutant androgen receptor protein. *J. Neurosci.*, **23**, 2203–2211.
37. Hegde, A.N. and Upadhya, S.C. (2007) The ubiquitin-proteasome pathway in health and disease of the nervous system. *Trends Neurosci.*, **30**, 587–595.
38. Wyttenbach, A., Carmichael, J., Swartz, J., Furlong, R.A., Narain, Y., Rankin, J. and Rubinsztein, D.C. (2000) Effects of heat shock, heat shock protein 40 (HDJ-2), and proteasome inhibition on protein aggregation in cellular models of Huntington's disease. *Proc. Natl Acad. Sci. USA*, **97**, 2898–2903.
39. Davies, S.W., Turmaine, M., Cozens, B.A., DiFiglia, M., Sharp, A.H., Ross, C.A., Scherzinger, E., Wanker, E.E., Mangiarini, L. and Bates, G.P. (1997) Formation of neuronal intranuclear inclusions underlies the neurological dysfunction in mice transgenic for the HD mutation. *Cell*, **90**, 537–548.
40. DiFiglia, M., Sapp, E., Chase, K.O., Davies, S.W., Bates, G.P., Vonsattel, J.P. and Aronin, N. (1997) Aggregation of huntingtin in neuronal intranuclear inclusions and dystrophic neurites in brain. *Science*, **277**, 1990–1993.
41. Yamamoto, A., Lucas, J.J. and Hen, R. (2000) Reversal of neuropathology and motor dysfunction in a conditional model of Huntington's disease. *Cell*, **101**, 57–66.
42. Zu, T., Duvick, L.A., Kaytor, M.D., Berlinger, M.S., Zoghbi, H.Y., Clark, H.B. and Orr, H.T. (2004) Recovery from polyglutamine-induced neurodegeneration in conditional SCA1 transgenic mice. *J. Neurosci.*, **24**, 8853–8861.
43. Lee, C.K., Weindruch, R. and Prolla, T.A. (2000) Gene-expression profile of the ageing brain in mice. *Nat. Genet.*, **25**, 294–297.
44. Keller, J.N., Huang, F.F. and Markesbery, W.R. (2000) Decreased levels of proteasome activity and proteasome expression in aging spinal cord. *Neuroscience*, **98**, 149–156.
45. Kamal, A., Thao, L., Sensintaffar, J., Zhang, L., Boehm, M.F., Fritz, L.C. and Burrows, F.J. (2003) A high-affinity conformation of Hsp90 confers tumour selectivity on Hsp90 inhibitors. *Nature*, **425**, 407–410.
46. Egorin, M.J., Zuhowski, E.G., Rosen, D.M., Sentz, D.L., Covey, J.M. and Eiseman, J.L. (2001) Plasma pharmacokinetics and tissue distribution of 17-(allylamino)-17-demethoxygeldanamycin (NSC 330507) in CD2F1 mice1. *Cancer Chemother. Pharmacol.*, **47**, 291–302.
47. Page, J., Heath, J., Fulton, R., Yalkowsky, E., Tabibi, E., Tomaszewski, J., Smith, A. and Rodman, L. (1997) Comparison of geldanamycin (NSC-122750) and 17-allylaminogeldanamycin (NSC-330507D) toxicity in rats. *Proc. Am. Assoc. Cancer Res.*, **38**, 308.
48. Supko, J.G., Hickman, R.L., Grever, M.R. and Malspeis, L. (1995) Preclinical pharmacologic evaluation of geldanamycin as an antitumor agent. *Cancer Chemother. Pharmacol.*, **36**, 305–315.
49. Wetzler, M., Earp, J.C., Brady, M.T., Keng, M.K. and Jusko, W.J. (2007) Synergism between arsenic trioxide and heat shock protein 90 inhibitors on signal transducer and activator of transcription protein 3 activity—pharmacodynamic drug-drug interaction modeling. *Clin. Cancer Res.*, **13**, 2261–2270.
50. Hollingshead, M., Alley, M., Burger, A.M., Borgel, S., Pacula-Cox, C., Fiebig, H.H. and Sausville, E.A. (2005) In vivo antitumor efficacy of 17-DMAG (17-dimethylaminoethylamino-17-demethoxygeldanamycin hydrochloride), a water-soluble geldanamycin derivative. *Cancer Chemother. Pharmacol.*, **56**, 115–125.
51. Shadad, F.N. and Ramanathan, R.K. (2006) 17-dimethylaminoethylamino-17-demethoxygeldanamycin in patients with advanced-stage solid tumors and lymphoma: a phase 1 study. *Clin. Lymphoma Myeloma*, **6**, 500–501.
52. Smith, M.A., Morton, C.L., Phelps, D.A., Kolb, E.A., Lock, R., Carol, H., Reynolds, C.P., Maris, J.M., Keir, S.T., Wu, J. *et al.* (2008) Stage 1 testing and pharmacodynamic evaluation of the HSP90 inhibitor alvespimycin (17-DMAG, KOS-1022) by the pediatric preclinical testing program. *Pediatr. Blood Cancer*, **51**, 34–41.
53. Egorin, M.J., Rosen, D.M., Wolff, J.H., Callery, P.S., Musser, S.M. and Eiseman, J.L. (1998) Metabolism of 17-(allylamino)-17-demethoxygeldanamycin (NSC 330507) by murine and human hepatic preparations. *Cancer Res.*, **58**, 2385–2396.

54. Zhang, Y.Q. and Sarge, K.D. (2007) Celastrol inhibits polyglutamine aggregation and toxicity though induction of the heat shock response. *J. Mol. Med.*, **85**, 1421–1428.
55. Sittler, A., Lurz, R., Lueder, G., Priller, J., Lehrach, H., Hayer-Hartl, M.K., Hartl, F.U. and Wanker, E.E. (2001) Geldanamycin activates a heat shock response and inhibits huntingtin aggregation in a cell culture model of Huntington's disease. *Hum. Mol. Genet.*, **10**, 1307–1315.
56. Katsuno, M., Sang, C., Adachi, H., Minamiyama, M., Waza, M., Tanaka, F., Doyu, M. and Sobue, G. (2005) Pharmacological induction of heat-shock proteins alleviates polyglutamine-mediated motor neuron disease. *Proc. Natl Acad. Sci. USA*, **102**, 16801–16806.
57. Bailey, C.K., Andriola, I.F., Kampinga, H.H. and Merry, D.E. (2002) Molecular chaperones enhance the degradation of expanded polyglutamine repeat androgen receptor in a cellular model of spinal and bulbar muscular atrophy. *Hum. Mol. Genet.*, **11**, 515–523.
58. Al-Ramahi, I., Lam, Y.C., Chen, H.K., de Gouyon, B., Zhang, M., Perez, A.M., Branco, J., de Haro, M., Patterson, C., Zoghbi, H.Y. *et al.* (2006) CHIP protects from the neurotoxicity of expanded and wild-type ataxin-1 and promotes their ubiquitination and degradation. *J. Biol. Chem.*, **281**, 26714–26724.
59. Adachi, H., Waza, M., Tokui, K., Katsuno, M., Minamiyama, M., Tanaka, F., Doyu, M. and Sobue, G. (2007) CHIP overexpression reduces mutant androgen receptor protein and ameliorates phenotypes of the spinal and bulbar muscular atrophy transgenic mouse model. *J. Neurosci.*, **27**, 5115–5126.
60. Dickey, C.A., Kamal, A., Lundgren, K., Klosak, N., Bailey, R.M., Dunmore, J., Ash, P., Shoraka, S., Zlatkovic, J., Eckman, C.B. *et al.* (2007) The high-affinity HSP90-CHIP complex recognizes and selectively degrades phosphorylated tau client proteins. *J. Clin. Invest.*, **117**, 648–658.
61. Auluck, P.K. and Bonini, N.M. (2002) Pharmacological prevention of Parkinson disease in Drosophila. *Nat. Med.*, **8**, 1185–1186.
62. Lu, A., Ran, R., Parmentier-Batteur, S., Nee, A. and Sharp, F.R. (2002) Geldanamycin induces heat shock proteins in brain and protects against focal cerebral ischemia. *J. Neurochem.*, **81**, 355–364.
63. Murphy, P., Sharp, A., Shin, J., Gavrilyuk, V., Dello Russo, C., Weinberg, G., Sharp, F.R., Lu, A., Heneka, M.T. and Feinstein, D.L. (2002) Suppressive effects of ansamycins on inducible nitric oxide synthase expression and the development of experimental autoimmune encephalomyelitis. *J. Neurosci. Res.*, **67**, 461–470.
64. Katsuno, M., Adachi, H., Doyu, M., Minamiyama, M., Sang, C., Kobayashi, Y., Inukai, A. and Sobue, G. (2003) Leuprorelin rescues polyglutamine-dependent phenotypes in a transgenic mouse model of spinal and bulbar muscular atrophy. *Nat. Med.*, **9**, 768–773.
65. Hamazaki, J., Iemura, S., Natsume, T., Yashiroda, H., Tanaka, K. and Murata, S. (2006) A novel proteasome interacting protein recruits the deubiquitinating enzyme UCH37 to 26S proteasomes. *EMBO J.*, **25**, 4524–4536.
66. Murata, S., Minami, Y., Minami, M., Chiba, T. and Tanaka, K. (2001) CHIP is a chaperone-dependent E3 ligase that ubiquitylates unfolded protein. *EMBO Rep.*, **2**, 1133–1138.
67. Minamiyama, M., Katsuno, M., Adachi, H., Waza, M., Sang, C., Kobayashi, Y., Tanaka, F., Doyu, M., Inukai, A. and Sobue, G. (2004) Sodium butyrate ameliorates phenotypic expression in a transgenic mouse model of spinal and bulbar muscular atrophy. *Hum. Mol. Genet.*, **13**, 1183–1192.
68. Adachi, H., Kume, A., Li, M., Nakagomi, Y., Niwa, H., Do, J., Sang, C., Kobayashi, Y., Doyu, M. and Sobue, G. (2001) Transgenic mice with an expanded CAG repeat controlled by the human AR promoter show polyglutamine nuclear inclusions and neuronal dysfunction without neuronal cell death. *Hum. Mol. Genet.*, **10**, 1039–1048.
69. Hirano, Y., Hayashi, H., Iemura, S., Hendil, K.B., Niwa, S., Kishimoto, T., Kasahara, M., Natsume, T., Tanaka, K. and Murata, S. (2006) Cooperation of multiple chaperones required for the assembly of mammalian 20S proteasomes. *Mol. Cell*, **24**, 977–984.
70. Hamazaki, J., Sasaki, K., Kawahara, H., Hisanaga, S., Tanaka, K. and Murata, S. (2007) Rpn10-mediated degradation of ubiquitinated proteins is essential for mouse development. *Mol. Cell. Biol.*, **27**, 6629–6638.
71. Menendez-Benito, V., Heessen, S. and Dantuma, N.P. (2005) Monitoring of ubiquitin-dependent proteolysis with green fluorescent protein substrates. *Methods Enzymol.*, **399**, 490–511.

B-type natriuretic peptide and cardiovalvulopathy in Parkinson disease with dopamine agonist

H. Watanabe, MD
M. Hirayama, MD
A. Noda, PhD
M. Ito, MD
N. Atsuta, MD
J. Senda, MD
T. Kaga, MD
A. Yamada, MD
M. Katsuno, MD
T. Niwa, MD
F. Tanaka, MD
G. Sobue, MD

Address correspondence and reprint requests to Dr. Gen Sobue, Department of Neurology, Nagoya University Graduate School of Medicine, Nagoya 466-8550, Japan
sobueg@med.nagoya-u.ac.jp

ABSTRACT

Objective: To elucidate the usefulness of plasma B-type natriuretic peptide (BNP) values for evaluating adverse effects of pergolide or cabergoline on cardiovalvulopathy in patients with Parkinson disease.

Methods: Twenty-five patients treated with pergolide or cabergoline (ergot group) and 25 patients never treated with ergot derivatives (non-ergot group) were enrolled. Plasma BNP values and detailed echocardiography were evaluated. Thirty age- and gender-matched controls were similarly evaluated.

Results: Patients with regurgitation more than grade 3 were more frequent in the ergot group than in the non-ergot group as well as control groups (24%, 0%, 3%, $p = 0.001$). Both composite regurgitation scores and plasma BNP values were significantly higher in the ergot group than in controls. In the ergot group, the cumulative dose correlated to both tenting area ($r = 0.57$, $p = 0.004$) and tenting distance ($r = 0.62$, $p = 0.001$). Furthermore, plasma BNP values were higher in patients with severe or multiple regurgitation groups ($p < 0.001$), and were correlated with composite regurgitation score ($r = 0.70$, $p < 0.001$). Multiple regression analyses revealed that BNP values were independently correlated with both composite regurgitation and left ventricular ejection fraction.

Conclusion: The combination of comprehensive echocardiography and plasma B-type natriuretic peptide levels elucidates the presence of cardiac damage in patients with Parkinson disease using ergot derivative dopamine agonists. ***Neurology*® 2009;72:621–626**

GLOSSARY

AR = aortic regurgitation; **BNP** = B-type natriuretic peptide; **MR** = mitral regurgitation; **PD** = Parkinson disease; **TR** = tricuspid regurgitation; **UPDRS** = Unified Parkinson's Disease Rating Scale.

Ergot derivative dopamine agonists including pergolide and cabergoline are some of the most effective drugs to treat parkinsonian symptoms and have the potential to reduce the motor complications observed in patients with Parkinson disease (PD) treated with L-dopa.[1] However, several reports have shown an association of ergot derivative dopamine agonists and cardiac multivalvular regurgitation.[2-18] In particular, high cumulative doses and long-term treatment with pergolide and cabergoline have been considered to be risk factors for increased valvulopathy in patients with PD. The US Food and Drug Administration public health advisory of March 29, 2007, cautions against abruptly stopping pergolide and is looking for ways to provide the drug to those people who cannot successfully switch to alternative treatments. On the contrary, over 60% of patients did not show valvulopathy, despite several years' exposure.[2] In Japan, similar to some European countries, pergolide and cabergoline are still used, and moderate doses of pergolide are associated with a low incidence of restrictive valvulopathy.[4,9]

From the Departments of Neurology (H.W., M.H., M.I., N.A., J.S., T.K., M.K., F.T., G.S.) and Cardiology (A.Y.), Nagoya University Graduate School of Medicine; and Departments of Medical Technology (A.N.) and Clinical Preventive Medicine (T.N.), Nagoya University School of Health Sciences, Japan.

Supported by Health and Labor Sciences Research grants for research on measures for intractable diseases and comprehensive research on Aging and Health of the Ministry of Health, Labor and Welfare, Japan.

Disclosure: The authors report no disclosures.

Although echocardiography is an essential tool to evaluate valvulopathy, a simple screening test that does not require specialized techniques would be beneficial for management of patients under various conditions in particular institutes without a department of cardiovascular medicine. B-type natriuretic peptide (BNP), which is secreted mainly from the heart and belongs to the natriuretic peptide family, is indicative of cardiac dysfunction in patients with not only heart failure and coronary artery disease but also valvular disorders.[19-21] Since plasma BNP values can be measured in serum by fully automated and commercially available assays with excellent test precision, it would be beneficial for monitoring the cardiac findings in patients with PD.

In this study, we investigated the usefulness of plasma BNP values for identifying and monitoring cardiac involvement in patients with PD treated with ergot derivative dopamine agonists.

METHODS The records of 121 patients with PD who attended the Department of Neurology, Nagoya University Hospital, and were nominated to our clinical cohort study at Nagoya area[22] during January to December 2006 were investigated. Of these, 34 patients with PD who fulfilled probable PD criteria according to the established diagnostic criteria[23] and were continuously taking ergot agonists (pergolide or cabergoline) but not non-ergot ones for a minimum of 1 year with or without levodopa were enrolled. Switching dopamine agonists between pergolide and cabergoline or combined use of pergolide and cabergoline often occurs in clinical practice. Although there are no controlled data for the comparison of two or more dopamine agonists to define equivalent dosages, several reports have been published on the clinical experience of experts.[24] In addition, the stimulus strength on 5-hydroxytryptamine 2B (5-HT_{2B}) receptors is similar between cabergoline and pergolide, in parallel with their molecular weights.[25,26] Thus, according to a previous report,[24] we calculated that 2 mg of pergolide is equal to 3 mg of cabergoline. Age- and sex-matched patients with PD who were never treated with ergot derivative dopamine agonists were also included. Six patients taking nonpermitted medication (anorectic or ergot alkaloid agents, Chinese herbs, anticancer or immune-suppressive drugs before enrollment), having a history of significant coronary heart disease, impaired function/dilatation of left/right ventricle, history of peripheral artery occlusive disease, and any clinically significant illnesses that may interfere with their capability to participate in the study were excluded. We also excluded three patients who were not treated in our institute because their history of taking dopamine agonists was found to be inaccurate. As a result, 25 patients treated with pergolide or cabergoline were enrolled in the ergot group. Thirteen patients were treated with pergolide or cabergoline. Five patients were only treated with pergolide and seven patients only with cabergoline. In addition, 25 patients never treated with ergot derivatives were also enrolled in the non-ergot group. Disease severity was assessed with the Unified Parkinson's Disease Rating Scale (UPDRS) and the Hoehn & Yahr stages. All patients showed normal renal function. Two of the ergot group and three of the non-ergot group patients had mild hypertension. Patients were interviewed with a structured questionnaire about the frequency of dyspnea, fatigue, leg edema, and palpitation, and were scored from 0 (no disability) to 4 (maximum). As for the controls, 30 age- and sex-matched normal volunteers who have no history of cardiac disorders and related conditions requiring medication were examined (age at examination: 67 ± 11 years; 16 women, 14 men). This study was approved by the ethics committee of Nagoya University Graduate School of Medicine. We obtained written informed consent from each participant before data collection.

All patients were assessed by an echocardiography GE VIVID 7 machine (GE Medical Systems, Milwaukee, WI) with two independent observers (A.N. and A.Y.) who were blinded to the clinical information. Mitral, aortic, and tricuspid valves were recorded from all possible views with the zoom function. In addition, a stethoscope examination was performed before echocardiography by A.N. and A.Y. Semiquantitative and quantitative measurements for quantification of regurgitant valvular diseases from the continuous wave, pulsed wave, and color Doppler examinations were assessed. Tenting distance and tenting area of the mitral valve were also evaluated as quantitative data.[7,8,10,15] We quantified regurgitant lesions by integration of all semiquantitative and quantitative measurements, and a final score was given as follows: absent, 0; trace, 1; mild, 2; moderate, 3; severe, 4.[27] A composite regurgitation score was calculated by adding the scores for aortic regurgitation (AR), mitral regurgitation (MR), and tricuspid regurgitation (TR).[7,13] The proportion of patients with any regurgitation grade from 3 to 4 was also assessed.[7] We derived the systolic pulmonary artery pressures from the TR jet, adding 10 mm Hg to the maximum gradient of the TR jet or 5 mm Hg if the vena cava inferior diameter was less than 10 mm with complete respiratory collapse and 15 mm Hg if the vena cava inferior was greater than 20 mm without respiratory variation. Left ventricular end-diastolic and end-systolic dimensions were measured, and the left ventricular ejection fraction was calculated by the Teicholz method. All patients with PD were investigated for both the diameter and flow of the hepatic vein and inferior vena cava using ultrasonography. In addition, a chest X-ray was also performed if necessary.

Blood for BNP quantification was collected in the fasting state in EDTA acid-treated tubes and placed on ice. After centrifugation at 2,500 rpm and 3°C, the plasma was stored at −80°C. BNP levels were measured directly with a specific immunoradiometric assay kit TOSOH AIA-PACK BNP (TOSOH Corp., Tokyo, Japan) including 30 age- and gender-matched controls.

Statistical analyses were performed using SPSS 15.0 for Windows (SPSS Inc.). Comparisons of age and disease duration between groups were performed using one-way analysis of variance followed by post hoc Bonferroni correction. Group comparisons of frequencies of valvular regurgitation were restricted to grades 3 and 4 and were performed using the Fisher exact test. The statistical threshold for post hoc comparisons between each treatment group vs the control group was set at $p < 0.017$ (0.05/3). The relationships between the cumulative dose of ergot derivative dopamine agonists and tenting area, tenting distance, composite regurgitation score, and BNP were analyzed using Pearson correlation test. Statistical significance was considered as $p < 0.05$.

RESULTS **Patient characteristics.** Patient characteristics were as follows: 22 men and 28 women; age at

examination, 66 ± 9 years; duration, 11.8 ± 9.6 years; mean Hoehn & Yahr stage 2.8. There were no significant differences between the ergot group and the non-ergot group in terms of Hoehn and Yahr staging (3.0 ± 0.9 vs 2.6 ± 0.9), duration of illness (12.9 ± 9.1 vs 10.6 ± 10.2 years), dosages of levodopa (494 ± 216 mg vs 481 ± 257 mg), age at examination (64.9 ± 9.2 vs 66.4 ± 7.7 years), and gender. Mean daily/cumulative dosage of pergolide was 1.1 ± 0.4/1,752 ± 1,512 mg and that of cabergoline was 3.1 ± 1.0/14,230 ± 2,566 mg. There were no patients who required a surgical operation during the course of this study. The frequency of leg edema, dyspnea, palpitation, and fatigue were not significantly different between the ergot group and the non-ergot group. All patients demonstrated more than 50% ejection fraction and did not show heart failure fulfilling the criteria of the Framingham study.[28,29]

Echocardiographic findings and plasma BNP levels. With respect to regurgitation, frequencies of equal to or greater than grade 3 regurgitation were only observed in the ergot group (12%, aortic valve; 12%, mitral valve; and 8%, tricuspid valve), except for one subject in the control group. The frequency of any grade 3 to 4 regurgitation was significant between the ergot group and non-ergot group as well as the ergot group and control group (ergot group vs non-ergot group; $p < 0.001$, ergot group vs control group; $p < 0.001$). Composite regurgitation scores in the ergot group were higher than in the control group ($p < 0.001$), but there were no differences between the ergot group and non-ergot group as well as between the non-ergot group and control group. Differences of tenting area and tenting distance between the ergot group and non-ergot group were slight (tenting area; ergot group, 1.26 ± 0.42, non-ergot group, 1.05 ± 0.21, $p = 0.04$, tenting distance; ergot group, 7.53 ± 2.57, non-ergot group, 6.10 ± 1.65, $p = 0.09$).

The plasma BNP levels as well as the composite regurgitation score were elevated in the ergot group vs the control group ($p = 0.004$, $p < 0.001$) (table). The BNP levels and composite regurgitation score in the ergot group showed a tendency to be increased as compared to those in the non-ergot group but did not show a significant difference. The BNP levels and composite regurgitation score in the non-ergot group were slightly elevated compared to control, although there was no significant difference.

Relationship between cumulative dose of ergot derivative dopamine agonists and echocardiographic findings. The cumulative dose of ergot derivative dopamine agonists was related to tenting distance ($r = 0.62$, $p = 0.001$) as well as to tenting area ($r = 0.57$, $p = 0.004$) but did not show any relationship with the composite regurgitation score ($r = 0.36$, $p = 0.08$). Within the high dose group (more than 4,000 mg), 33.3% of patients showed grade 3 to 4 regurgitation, while 15.4% of the low dose group (less than 4,000 mg) exhibited similar grades.

Plasma BNP levels in patients with severe valvulopathy. Plasma BNP values were higher in the ergot patient group with grade 3 to 4 regurgitation, which were seen only in the ergot group, than in those without such a high grade of regurgitation in the ergot group as well those in the non-ergot group (65.3 ± 47.8 pg/mL vs 24.7 ± 17.1 pg/mL vs 21.1 ± 15.4 pg/mL, $p < 0.001$). Patients with multiple regurgitation equal to or greater than grade 2 also had higher BNP values than those without (57.8 ± 46.1 vs 22.5 ± 11.9 vs 21.1 ± 15.4 pg/mL, $p < 0.001$).

According to receiver operating characteristic curve analyses to determine the adequate values for discriminating patients with severe regurgitation from those without, the most appropriate cutoff level of plasma BNP was 39.6 pg/mL, which showed 67.4% sensitivity and 84.4% specificity. In the ergot group, the positive predictive value was 66.7% and the negative predictive value was 89.4% if the plasma BNP level of 39.6 pg/mL was determined as the cutoff value.

Relationship between BNP and echocardiographic findings. The BNP levels showed a correlation to the composite regurgitation scores ($r = 0.70$, $p < 0.001$, figure) and a correlation to the left ventricular ejection fraction ($r = -0.42$, $p < 0.04$) but not age at examination, motor examination section (part III) of the UPDRS, and disease duration. Multiple regression analyses demonstrated that BNP values were independently correlated with composite regurgitation scores ($t = 4.08$, $p = 0.001$) and the left ventricular ejection fraction ($t = -2.07$, $p = 0.045$, $R^2 = 0.60$).

DISCUSSION We demonstrated that a significant elevation of plasma BNP values was observed in the ergot group vs in control groups. In particular, the BNP values were significantly elevated in the ergot group with more severe or multiple regurgitation than those with no to mild regurgitation and those in the non-ergot group. Furthermore, composite scores of regurgitation were well correlated with BNP values. Serum BNP is elevated in patients with valvular disorders due to ventricular pressure and volume load,[20,21] and this may be one reason why plasma BNP values increased in the ergot group. More recently, animal models have demonstrated that left ventricular cardiomyocytes were hypertrophic in both serotonin and pergolide-treated animals com-

Table Valvular abnormalities and plasma BNP values in the ergot group and non-ergot group

Grade of regurgitation, no. (%) of patients	Ergot group (n = 25)	Non-ergot group (n = 25)	Control (n = 30)
Aortic regurgitation			
0 to 1	13 (60)	22 (88)	27 (90)
2	7 (28)	3 (12)	3 (10)
3	2 (8)	0 (0)	0 (0)
4	1 (4)	0 (0)	0 (0)
Mitral regurgitation			
0 to 1	13 (60)	18 (72)	26 (87)
2	7 (28)	7 (28)	3 (10)
3	3 (12)	0 (0)	1 (3)
4	0 (0)	0 (0)	0 (0)
Tricuspid regurgitation			
0 to 1	19 (76)	21 (84)	25 (83)
2	4 (16)	4 (16)	5 (17)
3	1 (4)	0 (0)	0 (0)
4	1 (4)	0 (0)	0 (0)
Any grade from 3 to 4 regurgitation, mean (SD)	6 (24)*	0 (0)	1 (3)
Composite regurgitation score	3.30 (2.31)†	2.39 (1.29)	1.73 (1.83)
BNP (pg/mL)	33.6 (31.8)‡	21.1 (15.4)	14.2 (8.3)

Composite regurgitation score is the sum of mitral, aortic, and tricuspid regurgitation scores.
* The frequency of any grade 3 to 4 regurgitation was statistically significant between the ergot group and the non-ergot group ($p < 0.0001$) as well the ergot group and the control group ($p < 0.001$).
† Composite regurgitation score in the ergot group was significantly higher than that in the control group ($p < 0.001$). Composite regurgitation score of the ergot group tended to be increased when compared to the non-ergot group, but was not significantly different. Patients with grade 3 to 4 regurgitation were seen only in the ergot group.
‡ The plasma BNP level was significantly elevated in the ergot group vs in the control group ($p = 0.004$). The plasma BNP level of the ergot group tended to be increased when compared to the non-ergot group, but was not significantly different. The plasma BNP of patients with grade 3 to 4 regurgitation seen only in the ergot group was significantly elevated.
BNP = B-type natriuretic peptide.

Figure Correlation between composite regurgitation scores and serum B-type natriuretic peptide (BNP) values

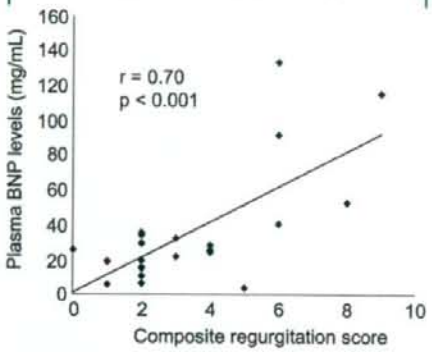

Composite regurgitation scores were correlated with BNP values ($r = 0.70$, $p < 0.001$). Composite regurgitation score was calculated by adding the score of aortic regurgitation, mitral regurgitation, and tricuspid regurgitation.

pared with placebo-treated animals, and macroscopically, left ventricular cavities were more dilated in both the serotonin and pergolide groups.[30] Thus, the second possible explanation is that direct toxic effects on the cardiomyocytes may have an influence on increased plasma BNP values. Since ventricular involvement in patients with PD using ergot derivative dopamine agonists has not been fully assessed, further prospective and pathologic studies will be needed to clarify this issue.

BNP is expected to detect preclinical structural and functional myocardial alterations not detectable by current techniques. Thus, BNP testing for structural heart disease screening in community-based populations is useful for cohorts with a high prevalence of heart disease.[31,32] However, age, renal dysfunction, and fluid overload can also contribute to elevated BNP concentrations.[33] Furthermore, elderly hypertensive subjects with orthostatic systolic blood pressure decrease also show significantly higher BNP values than in the control group, suggesting greater cardiac burden although the influence of orthostatic hypotension on BNP is not well known.[34] In this study, no patients exhibited symptomatic orthostatic hypotension but sympathetic dysfunction in PD might result in a slight elevation of plasma BNP levels in the non-ergot group compared with controls. Since ergot derivative dopamine agonists can exacerbate not only cardiac fibrosis but also renal dysfunction and orthostatic hypotension, measurement of plasma BNP values may be beneficial to detect and prevent the worsening of these clinical conditions by means of administration of such dopamine agonists.

This study showed that plasma BNP values were significantly higher in the ergot group than in controls, while the plasma BNP values showed a tendency to be elevated in the ergot group vs the non-ergot group, but did not show a significant difference. In this study, over three-quarters of patients in the ergot group did not develop significant valvular regurgitation. Such a low occurrence of severe valvulopathy may be a consequence of the lower dose of pergolide and cabergoline prescribed to our Japanese patients when compared to Western countries.[2,9] However, six patients of the ergot group with grade 3 to 4 regurgitation clearly showed a significant elevation of plasma BNP values compared to those of the non-ergot group. These results demonstrate that plasma BNP values can be used as a marker for patients who have reached a significant degree of heart valve involvement prior to heart failure.

This study also showed that the composite regurgitation score in the non-ergot group showed a slight elevation when compared to controls. We cannot rule out the possibility that other drugs including L-dopa or sympathetic dysfunction have an influence on the increase of regurgitation in the non-ergot group, but no patients with grade 3 to 4 regurgitation were observed in this group. According to a recent review, a considerably large proportion of patients do not develop valvulopathy, despite several years' exposure to high doses of pergolide, suggesting the presence of patients with a low susceptibility to pergolide.[2] Furthermore, the low dose of pergolide used in Japan can be associated with the low frequency of severe valvulopathy in our patients treated with ergot as mentioned above.[2,9] The striking point here is, as mentioned above, patients with a grade 3 to 4 composite score were present in the ergot group but not in the non-ergot group.

Both pergolide and cabergoline are potent agonists of not only dopamine but also the 5-HT_{2B} receptor. It is supposed that stimulation of 5-HT_{2B}, which is expressed in heart valves, induces prolonged activation of fibroblast mitogenesis resulting in valvular fibroplasia.[35,36] Thus, high dose and long-term ergot derivative administration is thought to be a risk factor for valvulopathy in patients with PD.[2-18] The significant association of the cumulative dose of ergot derivatives and mitral valve tenting area/distance, which have been proposed as restrictive changes due to valvular fibroplasia, was observed.[7,8,10,15] However, these significant adverse events did not occur in all ergot patients, including those administered high cumulative doses as previously reported,[2] suggesting that patients who receive benefit from ergot-derived dopamine agonists without valvulopathy will exist at a constant rate under careful follow-up.

In Germany, if any abnormalities are seen on echocardiography, non-ergot dopamine agonists are recommended.[37] Although there has been no report concerning plasma BNP values in patients with PD, our results support the view that plasma BNP levels will be a beneficial marker for monitoring cardiac fibrosis due to ergot derivative dopamine agonists. Measurement of plasma BNP levels is quicker, more accessible, and cheaper than echocardiography and may contribute to the assessment of not only the development of valvulopathy and myocardium damage but also several other important factors deteriorated by ergot derivative dopamine agonists in patients with PD. In addition, plasma BNP values can predict the prognosis of patients with chronic heart failure[38] and mitral regurgitation.[39] Echocardiography is effective and able to identify valvulopathy as a cause of incipient or present right heart failure, and it is a satisfactory screen for valvulopathy itself, but BNP is a suitable marker for the relevant forms of cardiac dysfunction. The combination of comprehensive echocardiography and plasma BNP levels will complementarily elucidate the presence of cardiac damage in patients with PD using ergot derivative dopamine agonists.

Received May 23, 2008. Accepted in final form November 17, 2008.

REFERENCES

1. Nutt JG, Wooten GF. Clinical practice: diagnosis and initial management of Parkinson's disease. N Engl J Med 2005;353:1021–1027.
2. Antonini A, Poewe W. Fibrotic heart-valve reactions to dopamine-agonist treatment in Parkinson's disease. Lancet Neurol 2007;6:826–829.
3. Corvol JC, Anzouan-Kacou JB, Fauveau E, et al. Heart valve regurgitation, pergolide use, and Parkinson disease: an observational study and meta-analysis. Arch Neurol 2007;64:1721–1726.
4. Růzicka E, Línková H, Penicka M, Ulmanová O, Nováková L, Roth J. Low incidence of restrictive valvulopathy in patients with Parkinson's disease on moderate dose of pergolide. J Neurol 2007;254:1575–1578.
5. Dewey RB 2nd, Reimold SC, O'Suilleabhain PE. Cardiac valve regurgitation with pergolide compared with nonergot agonists in Parkinson disease. Arch Neurol 2007;64:377–380.
6. Schade R, Andersohn F, Suissa S, Haverkamp W, Garbe E. Dopamine agonists and the risk of cardiac-valve regurgitation. N Engl J Med 2007;356:29–38.
7. Zanettini R, Antonini A, Gatto G, Gentile R, Tesei S, Pezzoli G. Valvular heart disease and the use of dopamine agonists for Parkinson's disease. N Engl J Med 2007;356:39–46.
8. Junghanns S, Fuhrmann JT, Simonis G, et al. Valvular heart disease in Parkinson's disease patients treated with dopamine agonists: a reader-blinded monocenter echocardiography study. Mov Disord 2007;22:234–238.
9. Yamamoto M, Uesugi T, Nakayama T. Dopamine agonists and cardiac valvulopathy in Parkinson disease: a case-control study. Neurology 2006;67:1225–1229.
10. Kim JY, Chung EJ, Park SW, Lee WY. Valvular heart disease in Parkinson's disease treated with ergot derivative dopamine agonists. Mov Disord 2006;21:1261–1264.
11. Peralta C, Wolf E, Alber H, et al. Valvular heart disease in Parkinson's disease vs. controls: An echocardiographic study. Mov Disord 2006;21:1109–1113.
12. Waller EA, Kaplan J, Heckman MG. Valvular heart disease in patients taking pergolide. Mayo Clin Proc 2005;80:1016–1020.
13. Baseman DG, O'Suilleabhain PE, Reimold SC, Laskar SR, Baseman JG, Dewey RB Jr. Pergolide use in Parkinson disease is associated with cardiac valve regurgitation. Neurology 2004;63:301–304.
14. Horvath J, Fross RD, Kleiner-Fisman G, et al. Severe multivalvular heart disease: a new complication of the ergot derivative dopamine agonists. Mov Disord 2004;19:656–662.